

Efficiency of weak lensing surveys to probe cosmological models

L. van Waerbeke^{1,2,3}, F. Bernardeau⁴, Y. Mellier^{5,6}

¹ CITA, 60 St Georges Str., Toronto, M5S 3H8 Ontario, Canada.

² MPA, Karl-Schwarzschild-Str. 1, Postfach 1523, D-85740 Garching, Germany.

³ OMP, 14 av. Edouard Belin, 31400, Toulouse, France.

⁴ Service de Physique Théorique. C.E. de Saclay. 91191 Gif-sur-Yvette Cedex, France.

⁵ Institut d'Astrophysique de Paris. 98 bis, boulevard Arago. 75014 Paris, France.

⁶ Observatoire de Paris. DEMIRM. 61, avenue de l'Observatoire. 75014 Paris, France.

May 25, 2022

Abstract. We apply a mass reconstruction technique to large-scale structure gravitational distortion maps, simulated for different cosmological scenarii on scales from 2.5 arcmin to 10 degrees. The projected mass is reconstructed using a non-parametric least square method involving the reduced shear on which noise due to intrinsic galaxy ellipticities has been added. The distortion of the galaxies is calculated using the full lens equation, without any hypothesis like the weak lensing approximation, or other linearization.

It is shown that the noise in the reconstructed maps is perfectly uncorrelated Poissonian, with no propagation from short to large scales. The measured power spectrum and first four moments of the convergence can be corrected accurately for this source of noise. The cosmic variance of these quantities is then analyzed with respect to the density of the background galaxies using 60 realizations of each model. We show that a moderately deep weak lensing survey (5×5 degrees with a typical background population of 30 gal/arcmin² at a redshift $z_s \simeq 1$) is able to probe the amplitude of the power spectrum with a few percent accuracy for models with $\sigma_8 \Omega^{0.8} = 0.6$.

Remarkably, we have found that, using the third moment of the local convergence only, such a survey would lead to a 6σ separation between open ($\Omega = 0.3$) and flat ($\Omega = 1$) models. This separation does not require a very deep survey, and it is shown to be robust against different hypothesis for the normalization or the shape of the power spectrum.

Finally, the observational strategy for an optimal measurement of the power spectrum and the moments of the convergence is discussed.

Key words: Cosmology: theory, dark matter, gravitational lenses, large-scale structure of Universe

1. Introduction

Mass reconstruction from gravitational distortion inversion is a promising technique to probe the mass distribution and the clustering on very large scales, regardless of the nature and the dynamical state of the dark and luminous matter. Pioneering theoretical work done by Gunn (1967), Jaroszyński et al. (1990), Blandford et al. (1991), Miralda-Escudé (1991) and Kaiser (1992) has shown that the expected distortion amplitude of weak lensing effects produced by large scale mass fluctuations (≥ 1 Mpc) is roughly at the percent level. This low level of distortion is observable due to the large number density of galaxies observed in deep surveys (Kaiser 1992). Needless is to say that the observation of such distortion fields provides a unique way to build a picture of the large scale mass distribution, independent on any biasing and/or dynamical prescriptions.

The scientific impact on the determination of cosmological parameters from weak lensing surveys has been underlined by recent theoretical work. Most of the papers quoted above show that the distortion two-point correlation function can be used to constrain the mass power spectrum. Villumsen (1996) remarked that the amplitude of the local distortion is proportional to the amplitude of the 3D density fluctuations *and* roughly to the density parameter Ω_0 . Bernardeau et al. (1997, hereafter BvWM) extended these calculations in the $\Omega_0 - \lambda$ plane and show that the amplitude is also slightly dependent on the cosmological parameter λ . In the same paper the authors also

show that the shape of the convergence probability distribution function can be used to disentangle the Ω and σ_8 dependence for models of large-scale structure formation with Gaussian initial conditions. In particular they demonstrate that the skewness¹, third moment expressed in terms of the square of the second, is roughly inversely proportional to the total mass density of the Universe Ω_0 , but independent on the amplitude of the fluctuations, as well as the shape of the power spectrum. This result, obtained by means of perturbation theory, is expected to be exact at large enough scale (see Gaztañaga & Bernardeau, 1998). The skewness should be enhanced in the nonlinear regime at small scales (Gaztañaga & Bernardeau 1998, see also Colombi et al. 1997, and Jain et al. 1998) which amplifies the differences between open and flat cosmologies. So, even if definitive quantitative predictions for such a quantity cannot be given from our present knowledge, it is clear that the skewness can accurately discriminate between different cosmological models.

Recently many theoretical and observational aspects have been investigated in detail in order to converge towards an unbiased measurement of such small distortions (Bonnet & Mellier 1995, Kaiser et al. 1995, and Van Waerbeke et al. 1997). The technical limitations that have been recognized so far come from systematics due to the correction of spurious distortions generated by the optic defects, fuzzy-shaped point spread function (PSF), and pixel convolution (sampling). Available image analysis techniques and image quality ensure that such systematics can now be reduced to a one percent level, which is necessary for these weak lensing applications, but beyond the need for cluster mass reconstruction. The ultimate limitation for the use of weak lensing surveys as a cosmological probe depends therefore on the accuracy with which the correction of the spurious distortions can be corrected. On the other hand, if the systematics can be reduced to the sub-percent level, the weak lensing analyses are limited by the intrinsic ellipticities of galaxies which acts as a shot noise for the gravitational distortion effect.

In this paper we investigate the effects of the shot noise and finite size survey (cosmic variance) on the determination of the cosmological parameters and the power spectrum. In particular, two goals are looked for,

- the precision on the determination of some cosmological parameters that can be expected from such maps;
- the maximum level of observational systematics which is acceptable in order to achieve these theoretical precisions.

This study is made in particular in the perspective of ongoing and future wide field deep imaging surveys devoted to weak lensing analysis (for instance the MEGACAM project, Boulade et al. 1998) at CFHT² or the SDSS

project, Stebbins 1996). In such a perspective, there are still open issues concerning the optimal observing strategy that should be adopted:

- Wide and shallow survey versus deep and narrow.
- The determination of the optimal shape and size of the survey depends on the noise properties, and on the correlation properties of the signal. The investigations that have been done so far (Kaiser 1992, 1998 and Seljak 1997) assume that the projected mass follows a Gaussian statistics. If such an assumption had to be dropped it may significantly change the conclusions that have been reached.

In addition, since the reconstruction of the projected mass from the shape of the galaxies is neither local nor linear in terms of the distortion field (Kaiser 1995) and of the intrinsic ellipticities of the galaxies, it is essential to understand how the noise propagates in the reconstructed mass maps. In order to investigate how these different effects may couple together, we built a series of projected mass maps that contain a realistic amount of non-Gaussianity. The associated distortion field is then derived on the basis of the full non-linear lens equation. A noise is added on the distortion maps, and the convergence is finally reconstructed. This paper presents the statistical analysis of those reconstructed maps for different cosmological models and different observational contexts.

The details of mass map generation and useful definitions are presented in Sect. 2. Sect. 3 presents the power spectrum analysis, the noise properties in the reconstructed mass maps, and the cosmic variance on the estimated power spectrum. Sect. 4 repeats similar analysis on moments in real space, where a comparison between top hat and compensated filter is done. It contains also some highlights about other possible statistical quantities that could be used to measure Ω , and a comparison with results obtained for different power spectra. We finally summarize our results and discuss the best observational strategies.

2. Generation of realistic κ -maps

2.1. Lensing effects, displacement and amplification matrix

Any mass concentration deflects light beams by an angle proportional to the gradient of the local gravitational potential. This effect induces an apparent displacement of the sources, so that a source that was at the angular position ξ^S will be observed at position ξ^I , with

$$\xi^S = \xi^I - \frac{2}{c^2} \frac{\mathcal{D}_K(\chi_s - \chi)}{\mathcal{D}_K(\chi)\mathcal{D}_K(\chi_s)} \int d\chi \nabla\phi(\chi, \xi^I), \quad (1)$$

where χ is the radial coordinate (χ_s is the one of the source), $\mathcal{D}_K(\chi)$ the co-moving angular diameter distance and $\phi(\chi, \xi)$ the 3D gravitational potential. The differential displacement of the images induces an image distortion,

¹ results are explicitly given at beginning of Sect. 4

² See also the WEB page http://terapix.iap.fr/terapix_megacam.html.

which depends on the second derivatives of the gravitational potential, i.e. on the mass density and the tidal field. This gravitational lensing effect of a thin lens is therefore characterized by an isotropic stretching, described by the convergence κ , and an anisotropic distortion given by the complex shear $\gamma = \gamma_1 + i\gamma_2$. The so-called amplification matrix \mathcal{A} describes the change of local coordinates between the source and image planes and can be written as

$$\mathcal{A} = \begin{pmatrix} 1 - \kappa - \gamma_1 & -\gamma_2 \\ -\gamma_2 & 1 - \kappa + \gamma_1 \end{pmatrix}. \quad (2)$$

Its elements are related to the first derivative of the displacement field,

$$\kappa = \frac{1}{2} (2 - \nabla \cdot \boldsymbol{\xi}^S) \quad (3)$$

$$\gamma_1 = \frac{1}{2} (\nabla_2 \xi_2^S - \nabla_1 \xi_1^S) \quad (4)$$

$$\gamma_2 = -\nabla_1 \xi_2^S, \quad (5)$$

and are therefore related to the projected gravitational potential of the lens ψ via,

$$\kappa = \Delta\psi/2; \quad \gamma_1 = (\psi_{11} - \psi_{22})/2; \quad \gamma_2 = \psi_{12}. \quad (6)$$

and where ψ is given by,

$$\psi(\boldsymbol{\varphi}, \chi_s) = \frac{2}{c^2} \int_0^{\chi_s} d\chi' \frac{\mathcal{D}_K(\chi - \chi')}{\mathcal{D}_K(\chi)\mathcal{D}_K(\chi')} \phi(\mathcal{D}_K(\chi')\boldsymbol{\varphi}, \chi'), \quad (7)$$

where $\boldsymbol{\varphi}$ is the angle such that $\boldsymbol{\xi} = \mathcal{D}_K(\chi)\boldsymbol{\varphi}$. Here ψ depends on χ_s since the potential is integrated from a given source plane χ_s to the observer. This can be trivially generalized to a source redshift distribution. This equation is valid only if the lens-lens coupling is dropped and the Born approximation is used. The validity of this assumption has been discussed by BvWM and Schneider et al. 1997 (hereafter SvWJK).

2.2. The galaxy shape matrices

A source galaxy may be described by a complex ellipticity defined as

$$\epsilon^{(s)} = \frac{1-r}{1+r} e^{2i\vartheta} \quad (8)$$

where ϑ is the galaxy orientation, and r is the square root of the ratio of the eigenvalues of the shape matrix $Q_{ij}^{(s)}$ of the (centered) surface brightness profile of the galaxy,

$$Q_{ij}^{(s)} = \int d\boldsymbol{\theta} \theta_i \theta_j \mathcal{S}(\boldsymbol{\theta}) / \int d\boldsymbol{\theta} \mathcal{S}(\boldsymbol{\theta}). \quad (9)$$

In presence of lensing, the shape matrix of the image of the galaxy is given by $Q = \mathcal{A}^{-1} Q^{(s)} \mathcal{A}^{-1}$, and provided that the amplification matrix does not vary over the galaxy's

area, the observed ellipticity is still described by Eq. (9), and it writes (Schneider & Seitz 1995),

$$\epsilon = \frac{\epsilon^{(s)} + g}{1 + g^* \epsilon^{(s)}}, \quad (10)$$

where $g = \gamma/(1 - \kappa)$ is the complex reduced shear. The observable is the distortion $\delta = 2g/(1 + |g|^2)$, but for sub-critical lenses like those we discuss in this work, g is also directly observable,

$$|g| = \sqrt{1/|\delta| - 1} - 1/|\delta|. \quad (11)$$

If the orientation of the source galaxies is random ($\langle \epsilon^{(s)} \rangle = 0$), the observed mean ellipticity of galaxies is an unbiased estimate of the reduced shear (Schramm & Kayser 1995, Schneider & Seitz 1995),

$$\langle \epsilon \rangle = g. \quad (12)$$

The weak lensing approximation ($\langle \epsilon \rangle \simeq \gamma$) is generally used in the case of lensing by large scale structures. However, we will not use that since we want to analyze the noise propagation in mass map reconstructed in the full non-linear regime (Eq. (10)).

2.3. Construction of the synthetic projected mass maps, and their reconstruction

The adopted procedure to build and analyze projected density maps is:

1) Generation of a density map, which directly provides the convergence κ given the source redshifts:

In order to make a precise analysis of the cosmic variance and noise properties in the reconstructed mass maps it is necessary to have a large set of simulations of large scale structure. Instead of CPU intensive N -body codes we use numerical fast second order Lagrangian dynamics (Moutarde et al. 1992) which has been shown to accurately reproduce the statistical properties of LSS (Munshi et al. 1994, Bernardeau et al. 1994, Bouchet et al. 1995). This allow us to build a large amount of projected mass maps for different cosmological models. The appendix A gives details about the generation of these maps and compares the non-Gaussian features with expectations from real dynamics.

2) Calculation of the associated reduced shear map g and addition of a given level of noise to the reduced shear map:

From the previous projected mass maps, a gravitational distortion map is computed, and the noise due to intrinsic ellipticities is added, as described in Appendix B. A "high" and "low" noise levels are simultaneously considered which correspond respectively to a mean number density of galaxies of $\bar{n} = 30$ gal/arcmin² and $\bar{n} = 50$ gal/arcmin². For the I-band, these number densities are

reachable with respectively 1.5 or 4.5 hours exposure at CFHT which is expected to provide galaxies of redshift of about unity. At this stage we have at our disposal a large number of maps that are supposed to mimic accurately what can be observed with large CCD cameras.

3) Reconstruction of the original κ map from ϵ :

Many mass reconstruction methods already exists (Seitz et al. 1998, Squires & Kaiser, 1996, and references therein). In this work, we use a non-parametric least square method (see Bartelmann et al. 1996 for details) which overfits data if no regularization process is used. The hope by doing so is to preserve all the noise properties intact, so that a detailed noise analysis can be done. The appendix B gives more technical details about the reconstruction algorithm.

Most of our generated images have an angular size of 5×5 degrees, 120×120 pixels, each pixel having a $2.5'$ angular side (hereafter, the *superpixel* size)³. These are typical scales that a MEGACAM survey at CFHT could probe. Images of size 10×10 degrees (240×240 pixels) have also been generated, in order to estimate how the cosmic variance depends on the survey size in the non-linear regime, and to compare the merit of deep-small survey area versus shallow-large survey. For each cosmological model and observational context series of 60 compact maps are produced. Table 1 summarizes the cases that investigated.

Table 1. List of simulations which have been carried out. The power spectrum BG corresponds to the formula (38). It is the same for $\Omega_0 = 1$ and $\Omega_0 = 0.3$. The CDM model corresponds to a standard CDM with $\Gamma = 0.5$. $\bar{\omega}$ is the ratio between the local convergence and the projected normalized density contrast, $\kappa = \bar{\omega} \delta_{2D}$ (see appendix A).

Spectrum	Ω_0	σ_8	z_{sources}	$\bar{\omega}$	size (deg ²)
BG	1.0	0.6	1.0	0.115	5×5
BG	0.3	1.53	1.0	0.045	5×5
BG	1.0	0.6	1.5	0.195	5×5
BG	0.3	1.40	1.5	0.0837	5×5
BG	1.0	0.6	1.0	0.115	10×10
BG	0.3	1.53	1.0	0.045	10×10
BG	1.0	1.0	1.0	0.115	5×5
sCDM	1.0	0.6	1.0	0.115	5×5

Fig. 1 shows two examples of initial κ maps, and the reconstructed mass of the noisy distortion maps. This panel illustrates what MEGACAM should be able to get during only 5 nights (!): 25 exposures in the I band, 1.5 hour each. A single MEGACAM field corresponds to a size of

³ The reason for that pixelisation is that second order Lagrangian dynamics is not able to probe high density peaks (i.e. small fields).

24×24 pixels on Fig. 1, which is clearly the required minimum area to detect large scale structure features like super clusters, filamentary structures or voids.

3. Power spectrum analysis of the reconstructed maps

3.1. Noise statistical properties of the reconstructed maps

It is clear that the mass reconstruction process does not produce any boundary effects (which is settled by definition). The only boundary effect, slightly detectable on the figure, is a larger level of noise at the edge of the field, due to the change in the finite difference scheme at that position (see Appendix B). The noise due to the intrinsic ellipticities of the galaxies is clearly visible at small scales.

Since the least χ^2 method used to reconstruct the convergence is a local process, it is unlikely that noise propagates on scales larger than the pixel size⁴.

Fig. 3 shows the power spectrum analysis of 60 reconstructed mass maps in the case of two different cosmological models $\Omega = 1$ (cases (a) and (b)) and $\Omega = 0.3$ (cases (c) and (d)). Fig. 3 (a) and (c) show the noise free power spectrum (solid lines) the power spectrum measured on the reconstructed maps with $\bar{n} = 30$ gal/arcmin² (dotted lines) and for $\bar{n} = 50$ gal/arcmin² (dashed lines). The plateau for the latter two cases is the consequence of the intrinsic ellipticities of the galaxies: at small scales, the power is dominated by the ellipticity of the galaxies, thus $P(k)$ tends to be constant, generally much higher than the signal. Figs. (b) and (d) show the difference of the power spectrum measurements on the reconstructed maps with the noise-free power spectrum; thin dotted line is for $\bar{n} = 50$ gal/arcmin² and thin dashed line for $\bar{n} = 30$ gal/arcmin². For visibility, error bars for scales larger than 20 arcmin have been dropped.

In 3D space, these angular scales correspond approximately to scales from 1 to 30 h^{-1} Mpc. We leave for later studies the problem of inverting the measured projected $P(k)$ to the 3D one. This aspect has already been explored at large angular scale by Seljak (1997).

As can be inferred from the power spectra in Figure 3, the noise has a flat power spectrum, characteristic of a white noise process. Fig. (2) illustrates the fact that the noise is independent on the underlying κ field and follows a Gaussian distribution. The noise model introduced by Kaiser (1998) based on the weak lensing approximation is now compared to the noise found in our simulations. The weak lensing approximation applied to Eq. (10) gives a local shear estimate $\hat{\gamma} = \gamma + \bar{\epsilon}^{(s)}$, where γ is the true shear and $\bar{\epsilon}^{(s)} = 1/N_p \sum \epsilon^{(s)}$, the mean intrinsic ellipticities of N_p galaxies in the superpixel p . Since the noise

⁴ This is less evident in the case of non-local mass reconstruction.

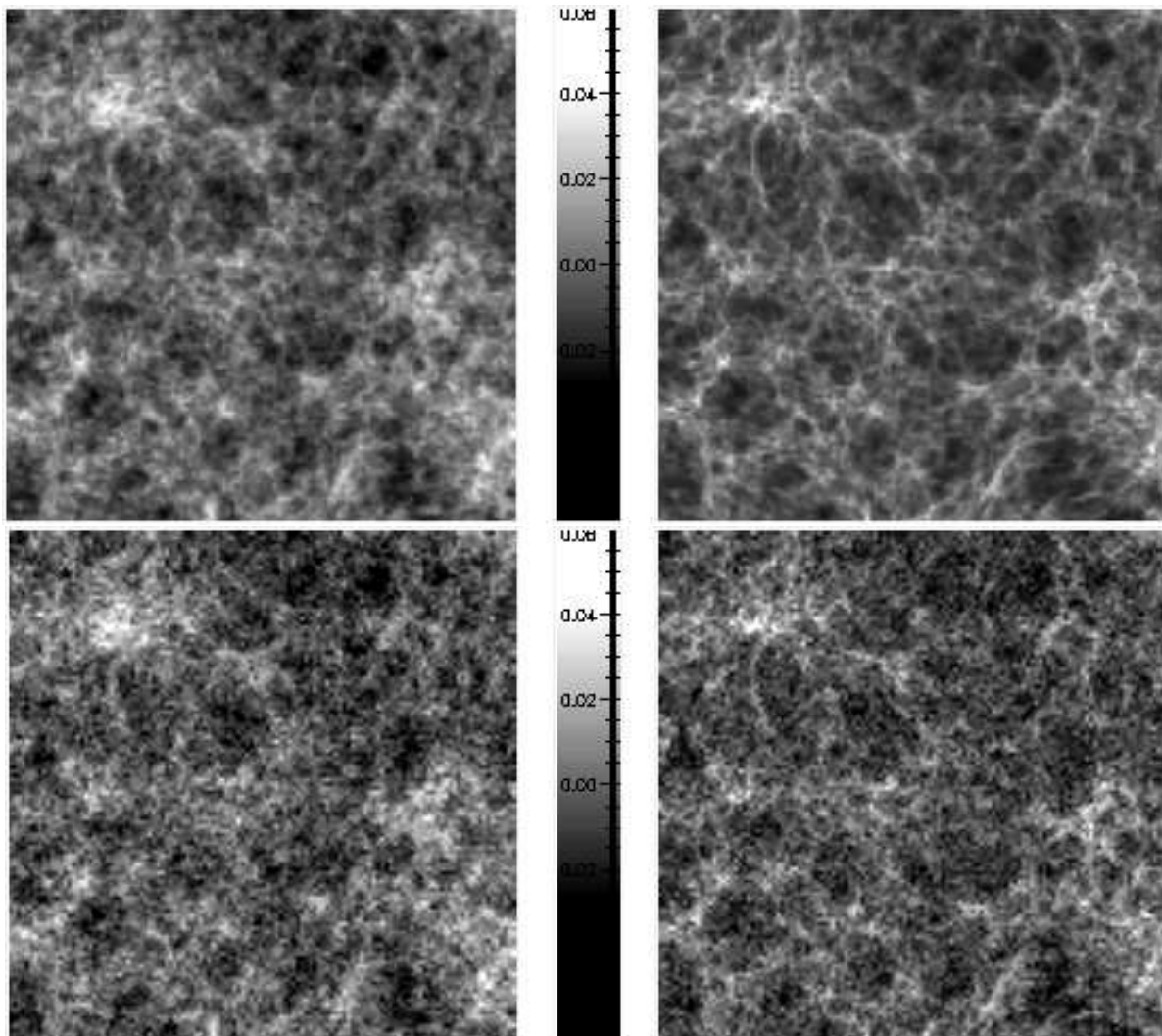


Fig. 1. Example of reconstructions of projected mass maps. The top panels show the initial noise-free κ map for either $\Omega = 1$ (left panel) or $\Omega = 0.3$ (right panel) with the same underlying linear random field (see Appendix A) and the same rms distortion. The bottom panels show the reconstructed κ maps with noise included in the shear maps. The maps cover a total area of 25 degrees². Each pixel has an angular size of 2.5 arcmin² and averages the shear signal expected from deep CCD exposures (about 30 galaxy/arcmin²). The sources are assumed to be all at redshift unity and to have an intrinsic ellipticity distribution given by Eq. (44). Such a survey is easily accessible to MEGACAM at CFHT. The precision with which the images can be reconstructed and the striking differences between the two cosmological models demonstrate the great interest such a survey would have.

components are assumed to be spatially uncorrelated, the statistical properties of the noise are,

$$\langle \bar{\epsilon}_\alpha^{(s)}(\boldsymbol{\theta}_i) \bar{\epsilon}_\beta^{(s)}(\boldsymbol{\theta}_j) \rangle = \sigma_\epsilon^2 \delta_{\alpha\beta}^K \delta_{ij}^K, \quad (13)$$

where $\alpha, \beta = (1, 2)$, δ^K is the Kronecker symbol and σ_ϵ is the variance of one component of the intrinsic ellipticities in one superpixel. The shear and the intrinsic ellipticities of the galaxies are uncorrelated in the weak lensing approximation. The measured power (on the noisy mass maps) can then be expressed only in terms of the true power $P_\kappa(\mathbf{k})$ (the one we want to estimate) and the power spectrum of the noise (Eq.(13)). If $\tilde{\kappa}$ denotes the Fourier

transform of the measured convergence, its power spectrum is given by

$$\langle \tilde{\kappa}^2(\mathbf{k}) \rangle \simeq \bar{n} P_\kappa(\mathbf{k}) + \bar{\sigma}_\epsilon^2. \quad (14)$$

This equation is only valid for a compact survey, where \bar{n} is the mean number density of the galaxies per superpixel, and $\bar{\sigma}_\epsilon$ is the mean value of σ_ϵ over the survey. For a sparse survey, the first term in Eq. (14) is changed into a convolution term, but the noise contribution to the observed

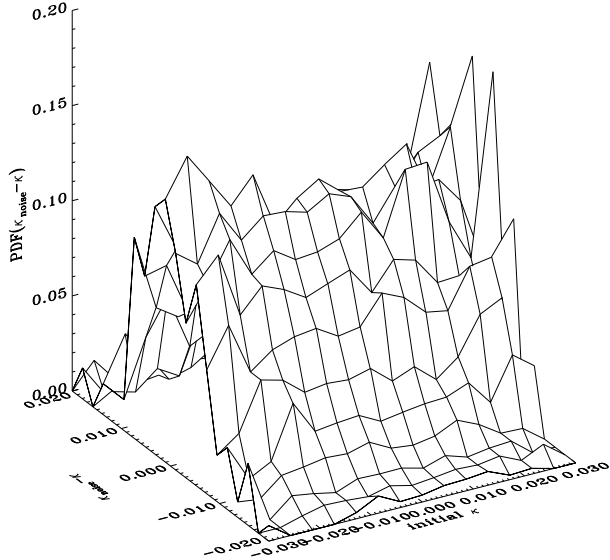


Fig. 2. Histograms of the difference between the noisy mass map and the initial mass map. The values of κ have been selected in bins. The histograms that are found to be all compatible with a Gaussian distribution with a fixed mean and width.

power spectrum remains independent on that power spectrum. A convenient way to estimate $\bar{\sigma}_\epsilon^2$ is to take

$$\bar{\sigma}_\epsilon^2 \simeq \frac{1}{n_{\text{pix}}} \sum_p \left(\frac{1}{N_p} \sum_{\text{gal}} [\epsilon_1^{(s)}]^2 \right), \quad (15)$$

where n_{pix} is the number of superpixels and N_p the number of galaxies in the superpixel p . This is nothing else but the variance of the observed ellipticities of the selected galaxies⁵.

The thin dashed and dotted straight lines on Fig. 3 correspond to the expected noise power spectra (for $\bar{n} = 30$ gal/arcmin² and $\bar{n} = 50$ gal/arcmin²) according to the Kaiser's model given by Eq. (14). It perfectly fits the noise part of the mass reconstructed with noisy data, whatever the cosmological model and the noise level. This is true even for the open cosmological models for which stronger non-linearities could have produced a stronger coupling with the noise. The fact that the noise component is pure white noise with an amplitude in agreement with the theoretical prediction is a remarkable result since the full non-linear equations were used, and it shows that the weak lensing approximation can be safely used to remove the noise component and to get an unbiased esti-

⁵ The noise depends only on the variance, not on higher moments of the intrinsic ellipticity distribution

mate of the power spectrum, down to the smallest scales considered here.

The behavior at scales smaller than our pixel size remains partly an open issue for two reasons: first, due to the smaller number of galaxies, the convergence of the reconstruction process as well as the stability of the noise properties has to be investigated. Second, at small scales the gravitational distortion is larger than only a few percent, and it can go up to infinity on the critical lines. Therefore, estimating the variance of the galaxies intrinsic ellipticity distribution, arcs and arclets should be removed. This issue can only be addressed in high resolution simulations like those performed by Jain et al. (1998).

3.2. Power spectrum cosmic variance

Although the estimate of the power spectrum described above is unbiased, the cosmic variance has also to be explored to come up with an optimal observational strategy.

In estimating the cosmic variance of the power spectrum, Gaussian statistics is usually assumed. This hypothesis is tested comparing the cosmic variance assuming Gaussian statistics to that of the simulated mass maps and that reconstructed using the two different level of noise defined before.

In the case of Gaussian statistics high order moment are related to the second order moments via the following relations:

$$\begin{aligned} \langle \tilde{\kappa}(\mathbf{k}_1) \dots \tilde{\kappa}(\mathbf{k}_{2p+1}) \rangle &= 0, \\ \langle \tilde{\kappa}(\mathbf{k}_1) \dots \tilde{\kappa}(\mathbf{k}_{2p}) \rangle &= \sum_{\text{perm } i=1}^p \prod \langle \tilde{\kappa}(\mathbf{k}_{2i-1}) \tilde{\kappa}(\mathbf{k}_{2i}) \rangle, \end{aligned} \quad (16)$$

which means that physically, the frequencies of a Gaussian field are not coupled, and that the $2p$ moment at a given frequency is only determined by the power at that frequency.

We consider a compact survey of size Θ , for which the number of modes available at a frequency is maximum. Thus, following Feldman et al. (1994) and Kaiser (1998), the cosmic variance $\sigma_{P_\kappa}^2(\mathbf{k})$ of $P_\kappa(\mathbf{k})$ is given by the square of the measured signal $\langle \tilde{\kappa}^2(\mathbf{k}) \rangle^2$ (which depends on $\bar{\sigma}_\epsilon$), divided by the number of independent modes used to determine it, $\Delta N(\mathbf{k})$ in the \mathbf{k} -annulus $(\mathbf{k}, \mathbf{k} + \Delta\mathbf{k})$. Simple modes count gives

$$\Delta N(\mathbf{k}) = \pi \frac{k \Delta k}{k_0^2}, \quad (17)$$

where $k_0 = 2\pi/\Theta$ is the fundamental frequency, thus

$$\sigma_{P_\kappa}(\mathbf{k}) = \frac{2\sqrt{\pi} \langle \tilde{\kappa}^2(\mathbf{k}) \rangle}{\Theta \sqrt{k \Delta k}}. \quad (18)$$

Note that in this hypothesis the cosmic variance is independent on the amplitude of the fluctuations. This is not

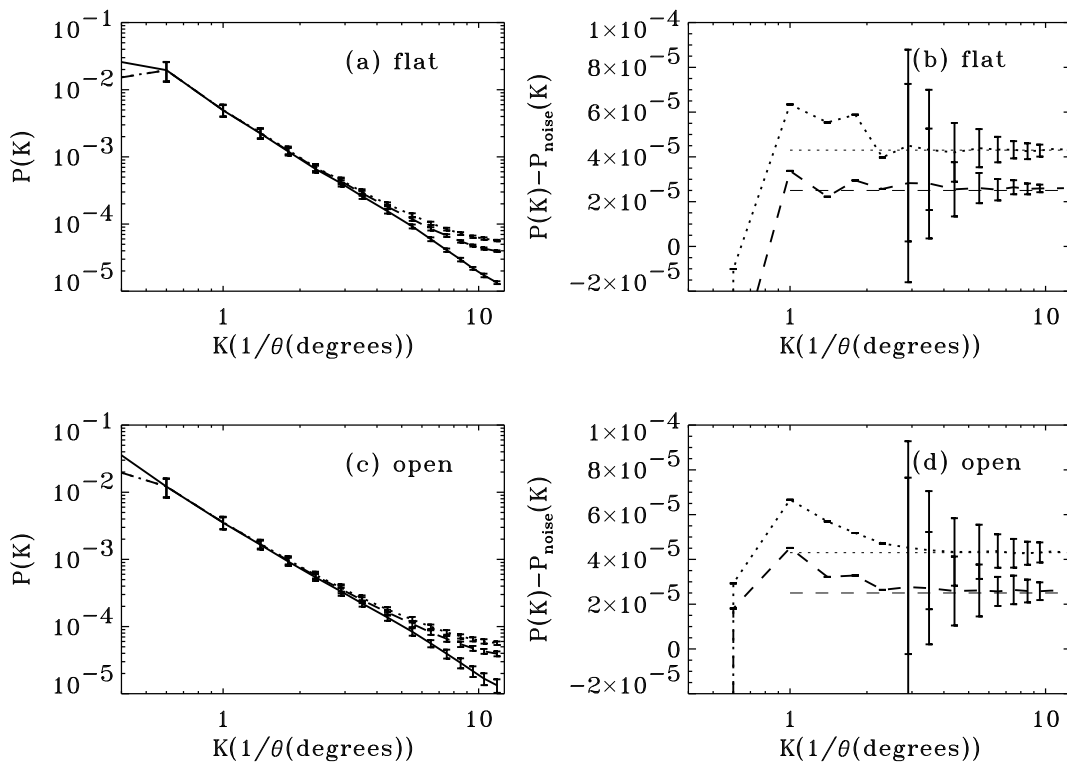


Fig. 3. Power spectrum analysis of the projected density field. The upper series of plots are for $\Omega = 1$ and the lower series for $\Omega = 0.3$. For all the plots, the solid lines show the power spectrum of the noise-free mass maps, before any mass reconstruction. The dotted lines correspond to the power spectrum estimation on the reconstructed noisy maps with a number density of galaxies of $\bar{n} = 30$ gal/arcmin², and the dashed lines for $\bar{n} = 50$ gal/arcmin². The left panels show the power spectrum estimates from the reconstructed noisy maps, compared to the true power spectrum. The right panels show the power contribution due to the noise, it is the difference of power spectra between the reconstructed noisy maps and the true power spectrum. The thin dashed and dotted straight lines show the expected value of the noise contribution in the simple linear noise model described by Eq.(14). It fits remarkably well the true noise level.

the case when the non-linear couplings are taken into account as it can be seen in Fig. 4. It shows the cosmic variance for flat ((a), (c), (e)) and open ((b), (d), (f)) cosmological models. (a) and (b) correspond to a 5×5 degree survey with $z_s = 1$, (c) and (d) with $z_s = 1.5$, and (e) and (f) a 10×10 degree survey with $z_s = 1$. On each plot, the thin solid line shows the Gaussian cosmic variance, the thick solid line shows the true cosmic variance without noise, the dotted line the noisy maps with $\bar{n} = 50$ gal/arcmin² and the dashed line with $\bar{n} = 30$ gal/arcmin². The vertical axis gives the error on the power spectrum measured at a given scale.

The departure from Gaussianity appears for scales below $10'$, the effect is however more important in the open case model for which non linearities are stronger. Open models ((b), (d), (f)) give almost the same features as for the flat models ((a), (c), (e)), although the cosmic variance is smaller. This is clearly a consequence of a higher power spectrum signal at low scales for these models, which is visible when comparing Fig. 3 (a) (flat) and

(c) (open). Thus, as expected, the intrinsic shape of the power spectrum affects the cosmic variance (Kaiser 1998).

Going deep in redshift (by comparing (a) and (c), or (b) and (d) for the open case) clearly improves the cosmic variance at small scale, since the gravitational distortion is stronger. However this stronger distortion does not improve the large scale power estimation because the cosmic variance at these scales only depends on the whole volume survey.

If shorter wave vectors are observed, (for a 10×10 degree survey), which is visualized on (e) and (f), a gain of 2 is reached at all scales, as a direct consequence of global increase of the number of modes in Eq.(17). For small scales, from the point of view of the statistics it is in fact equivalent to observe deep over a small area than to observe shallower over a large area (which reflects the fact that the dashed lines in (e) and (f) ($\bar{n} = 30$ gal/arcmin²) are almost the same as the dotted line in (a) and (b) ($\bar{n} = 50$ gal/arcmin²). But on the other hand, the shallow large survey gives a better estimate of the power at

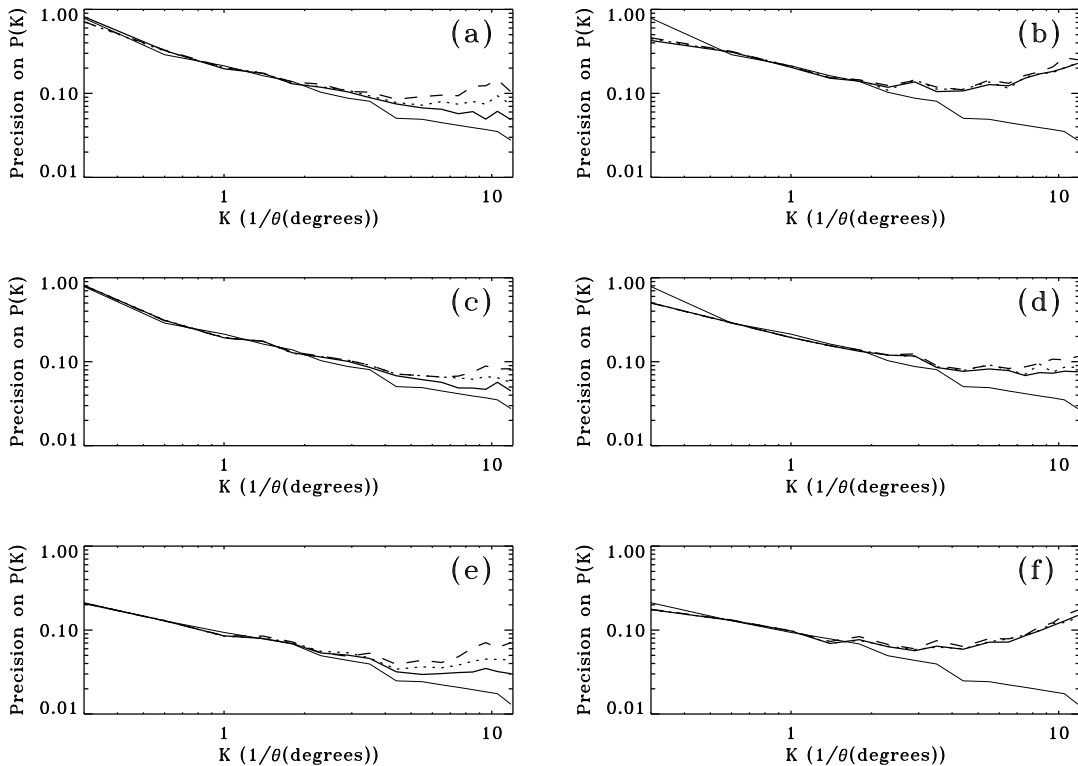


Fig. 4. Cosmic variance for flat (left panels) and open (right panels) models. The thin solid lines are the cosmic variance expected for a Gaussian density field given by Eq. (18). The thick solid lines show the true (measured on the simulations) cosmic variance. The dotted and dashed lines show the cosmic variance on the reconstructed mass maps, respectively with $\bar{n} = 50$ gal/arcmin² and $\bar{n} = 30$ gal/arcmin².

large scales than the deep survey. Since these two observational strategies require the same total exposure time it is clear that wide shallow surveys are better than small deep surveys. As it will be shown in Sect. 4, this remains true for the high order moments in real space. Moreover, deep surveys show more and more distant galaxies for which the redshift distribution is more uncertain.

4. Moments in real space

4.1. Signature of the normalization and non-Gaussian properties

Weak lensing carries more information than the amplitude and shape of the dark matter power spectrum. Fig. 1 demonstrates that distortion maps of the same amplitude (and with very similar power spectrum as can be checked in Fig. 2) can display very different features. On these maps the variance of the local convergence is the same, but the amount of non-linearities is very different. For low Ω universes, the same amount of distortion can be reached only with a rather large value of σ_8 thus corresponding to a much more evolved dynamics. As a result the difference between the underdense and the overdense regions

is more pronounced. The 'voids' tend to occupy a much larger area, whereas the super clusters tend to be sharper. These features appear because of the non-linear couplings contained in the gravitational dynamics. At large scale the use of Perturbation Theory has proved to be extremely good in predicting the emergence of such properties. All these calculations are based on the hypothesis that the initial conditions were Gaussian, which we will assume as well.

It has already been stressed (BvWM) that the departure from a Gaussian statistics is described by the skewness of the probability distribution function (PDF) of the local convergence. We will restrict our analysis on the skewness basically for two reasons: it is beyond the scope of this paper to explore all possible indicators of the non-Gaussian properties, and we know that the approximate dynamics we have adopted reproduces correctly the skewness of the local PDF (see Appendix A). In addition the lens-lens coupling and the Born approximation terms which are known to be small for the third moment are probably more important for higher orders, and this requires a complete dedicated work.

Let us summarize the expected results. For a top-hat window function we expect to have,

$$\sigma_\kappa \approx 0.01 \sigma_8 \Omega_0^{0.8} \left(\frac{\theta_0}{1 \text{deg.}} \right)^{-(n+2)/2} z_s^{0.75}, \quad (19)$$

$$s_3 \equiv \frac{\langle \kappa^3 \rangle}{\langle \kappa^2 \rangle^2} \approx 40 \Omega_0^{-0.8} z_s^{-1.35}, \quad (20)$$

where σ_κ is the rms value of κ at the scale θ_0 , n is the index of the power spectrum, σ_8 is the 3D rms density at $8h^{-1}\text{Mpc}$ scale and z_s is the mean redshift of the sources. The computed skewness s_3 is expected to be independent on the normalization of the power spectrum. It is only weakly dependent on the shape of the power spectrum as well as on the cosmological constant Λ (see discussion). The skewness would then be a very robust way⁶ of determining the density parameter Ω_0 .

Although the moment analysis is generally performed on the basis of a top-hat filter there is a priori no reason to limit our investigations to this filter. In particular SvWJK have proposed the use of an alternative function, the compensated filter that might prove more efficient to constrain Ω , with a lower cosmic variance.

4.2. Top-hat versus compensated filters

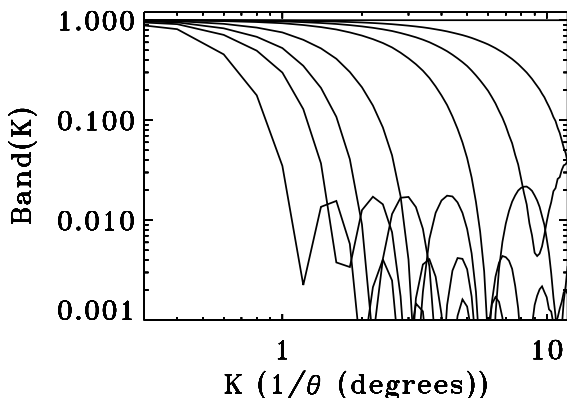


Fig. 5. Spectral response for the family of top-hat filters used in this work. The finite size effects are visible for the largest smoothing scales. The curves are not regularly spaced because of pixelisation effects.

Compensated filters were considered by SvWJK as a way to measure the convergence directly from the galaxy shape. They use the filter $V(\theta)$ of size θ_c that defines the quantity M_{ap} as

$$M_{\text{ap}}(\theta) = \int_0^{\theta_c} d^2\theta V(\theta) \gamma_t(\theta), \quad (21)$$

⁶ It is worth reminding that this is only possible if the redshift of the sources are perfectly known (which we assume here).

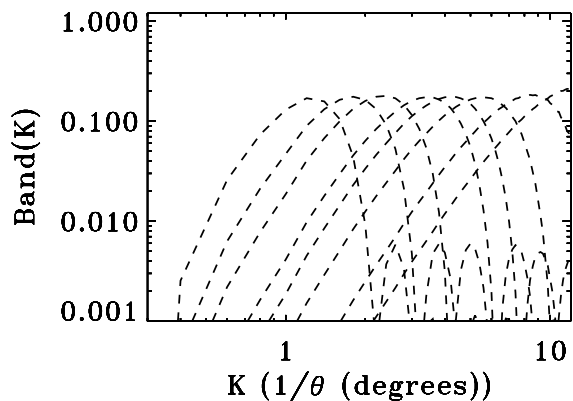


Fig. 6. Spectral response for the family of compensated filters used in this work.

where γ_t is the tangential component of the shear field. M_{ap} is the convergence field filtered by $U(\theta)$,

$$M_{\text{ap}}(\theta) = \int_0^{\theta_c} d^2\theta U(\theta) \kappa(\theta), \quad (22)$$

where $U(\theta)$ has to be the compensated filter and it is related to the arbitrary filter V through

$$V(\theta) = -U(\theta) + \frac{2}{\theta^2} \int_0^\theta d\theta' \theta' U(\theta'). \quad (23)$$

this latter filter is a compensated filter⁷ and, for instance, a convenient filter to use is given by,

$$U(\theta) = \frac{3}{\pi\theta_c} \left[1 - \left(\frac{\theta}{\theta_c} \right)^2 \right] \left[\frac{1}{3} - \left(\frac{\theta}{\theta_c} \right)^2 \right]. \quad (24)$$

The spectral responses (defined as the squared amplitude of the Fourier transforms of the window functions) of the filter's family used in this work are shown in Fig. 5 (for the top-hat) and by Fig. 6 (for the compensated filter $U(\theta)$). Clearly a field smoothed with a top-hat filter of size θ_c is sensitive to fluctuations of size larger than θ_c that contribute also to the cosmic variance of the moments. On the other hand, a compensated filter integrates the fluctuation modes only around the target frequency θ_c and any power at lower or larger scales will affect neither the signal nor its cosmic variance. SvWJK showed that the de-correlation properties of compensated filters are by far better than for top-hat filters because any power at small wavelengths between two disconnected fields is highly suppressed (see Fig. 8 of their paper). Thus the cosmic variance should be smaller for a compensated filter than for a top-hat filter.

⁷ A compensated filter is a filter with a vanishing mean value. This explains why M_{ap} can be measured only from the distortion field only since the mass-sheet degeneracy is removed by the used type of filters.

However this attractive feature comes with a price: a compensated filter needs to be sampled by a larger number of galaxies. In other words, the shot noise has a larger effect on the aperture mass M_{ap} than on the top-hat filtered mass at the same scale. A compromise has to be found, that depends on the functional shape of the compensated filter and on the shape of the power spectrum.

4.3. Moment estimations and shot noise corrections

Due to the intrinsic ellipticities of the galaxies and the cosmic variance (see for instance Szapudi & Colombi 1996, Colombi et al. 1998), estimates of the moments of κ from the reconstructed map are biased. We show here that the shot noise can be accurately calculated and the estimated moments corrected. It is worth noting that SvWJK has shown that we can find an unbiased estimator of the moments of M_{ap} , which completely cancel the shot noise correction problem. It is based on the measurement of the tangential shear γ_t . Unfortunately, the measurable quantity is g_t (the tangential reduced shear) rather than γ_t , and unless this is taken into account, the estimator given in SvWJK is no longer unbiased. In other words, the shot noise correction problem is shifted to an estimator correction problem.

It was shown in Section 3.1 that the shot noise leads to a pure white noise in the reconstructed convergence maps. The amplitude of this noise can be obtained by measuring the observed ellipticities of galaxies as described for the power spectrum estimation. Therefore, estimates of the variance and the skewness of the convergence in (19) and (20), corrected from the intrinsic ellipticities of the galaxies, are obtained by simply removing the noise term $\langle(\epsilon^{(s)})^2\rangle$ in the second moment. Note that the skewness correction only requires the correction of the variance since the third moment is not affected by the noise. As the analytical calculation of the noise term for compensated filters can be rather cumbersome, it is estimated using Monte-Carlo simulations.

Even after that noise correction, finite sample effects may bias the estimations of the second moment and of s_3 and may increase significantly the cosmic variance. This difficulty was partly investigated in BvWM with the use of perturbation theory. They pointed out that the accessible geometrical averages are expected to be smaller than the true ensemble averages, and that a dispersion is expected in the measurements (cosmic variance):

- the bias that affects the expectation values was found to be proportional to the variance at the sample size divided by the one of at the filtering scale;
- the scatter was found to be proportional to the rms of κ at the sample size.

These estimates were done fully in perturbation theory, with numerous approximations (in particular it was assumed that the sample size was much bigger than the

smoothing scale which is probably an erroneous approximation for most of the cases considered here). For accurate investigations of all these effects that take into account both the Poisson noise and the finite volume effects see Szapudi & Colombi (1996).

4.4. Results

We now turn to the measurement of moments in the simulated fields. The same simulations used for the power spectrum analysis are used here. The results are given in Figs. 7 (variance $\langle\kappa^2\rangle$ in a 5×5 degree field with $z_s = 1$) and 8 (skewness s_3 in a 5×5 degree field with $z_s = 1$). For each of these figures the plots are organized in the same way: the first row ((a), (b) and (c) plots) is for the flat model, the second row ((d), (e) and (f) plots) for the open model. It corresponds to the first two rows of Table 1. The first columns (a) and (d) show the estimator measured with a top-hat filter, the second columns (b) and (e) with a compensated filter, and the third columns (c) and (f) show the signal to noise ratio of these estimators. In plots (a), (b), (c) and (d) the solid lines give the estimators measured in the noise-free κ maps, the dotted lines in the noisy reconstructed maps with $\bar{n} = 50$ gal/arcmin² and the dashed lines with $\bar{n} = 30$ gal/arcmin². The dotted-dashed lines show the estimators measured on the reconstruction with noise with $\bar{n} = 30$ gal/arcmin² corrected from the noise. Since the case $\bar{n} = 50$ gal/arcmin² gives the same results they are not plotted. On the signal to noise plots (c) and (f) the thin solid lines show the results for a top-hat filter and the thick solid lines for a compensated filter. The results obtained for the noisy maps with $\bar{n} = 30$ gal/arcmin² or $\bar{n} = 50$ gal/arcmin² corrected from the noise are respectively given by the dashed and dotted lines (either thin or thick).

4.4.1. Noise correction

The noise correction as described in Sect 4.3 gives unbiased results, as it is expected for superimposed white noise. This is true even when the correction is two orders of magnitude higher than the signal (see for example Figs. 8 plots (b) and (e)). This confirms the simple properties of the noise in the reconstructed mass maps already found in Sect. 3.1.

4.4.2. The variance

The variance obtained for a top-hat filter is slowly decreasing with an increasing scatter, as expected. For the compensated filter the curves are almost flat as expected from the shape of the power spectrum. The noisy maps (dotted and dashed lines in Fig. 7.(a) and (b) display higher values for the variance. Once it is corrected, the results are in perfect agreement with the noise-free simulations. The signal to noise ratio is basically not affected by the shot noise

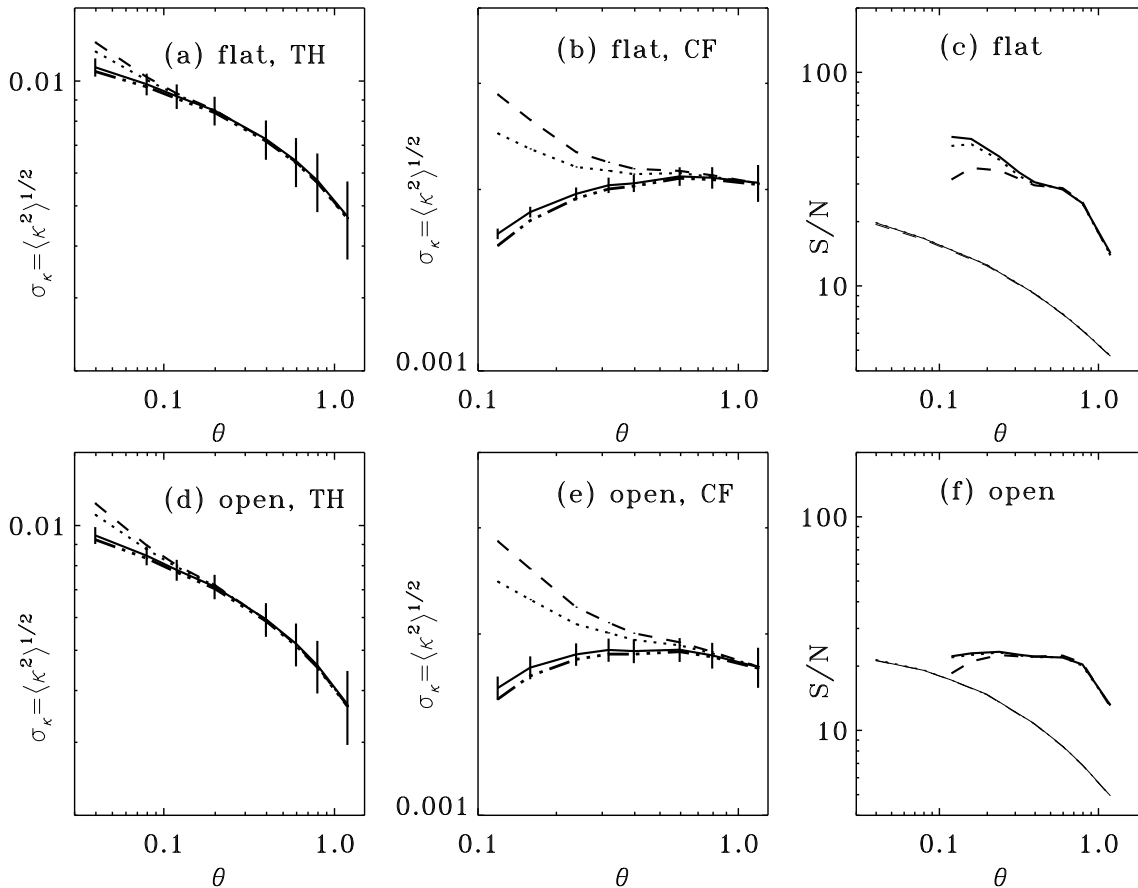


Fig. 7. The measured variance of the convergence, and the corresponding signal to noise ratio. The upper panels show the $\Omega = 1$ case, while the bottom panels correspond to the $\Omega = 0.3$ case. The left and middle panels are respectively the measured variance with a top-hat and a compensated filter. On these plots, the thick solid line is the true variance measured on the noise-free maps, the dashed line and the dotted line for the noisy reconstructed mass maps (with respectively $\bar{n} = 30$ gal/arcmin² and $\bar{n} = 50$ gal/arcmin²). The dotted-dashed line is the variance measured from the $n = 30$ gal/arcmin² case and corrected from the noise. The right panels show the signal to noise ratio of the variance detection with the top-hat (thin solid line) and compensated (thick solid line) filters. Dotted and dashed lines have the same meaning as for (a), (b), (d) and (e) but here the variance has been corrected from the noise.

for a top-hat filter, it shows that going deep does not improve the measurement precision. The compensated filter reveals much more sensitive to the shot noise as predicted in section 4.2 since we can see on plot Fig. 7. (c) and (f) (thick lines) the bell shape of the signal to noise ratio, with a significant reduction of the measurement precision at the smallest available scales. The open and flat cases show basically no differences. It can be seen however that the signal to noise ratio for a compensated filter is slightly lower for the open case. We interpret this effect as due to the presence of more nonlinear couplings in the maps. Remarkably, the precision with which the variance can be measured in some specific k range reaches 5%.

4.4.3. The skewness

The skewness can be accurately measured at the smallest scales (in Fig. 8 only the error bars for the first four points have been drawn). The skewness is decreasing with scale in the two cases. Once again, the noise correction applied to the reconstructed maps allow to recover the skewness with a surprising accuracy. The signal to noise of the skewness is still not affected by the noise for a top-hat filter, while for the compensated filter the situation is worse than for the variance; for instance, at the smallest scale, the signal to noise is almost one order of magnitude smaller on the reconstruction with noise than on the noise-free maps for the $\Omega = 1$ case. The two models, open and flat, provide us with very different magnitude for s_3 . Their skewness

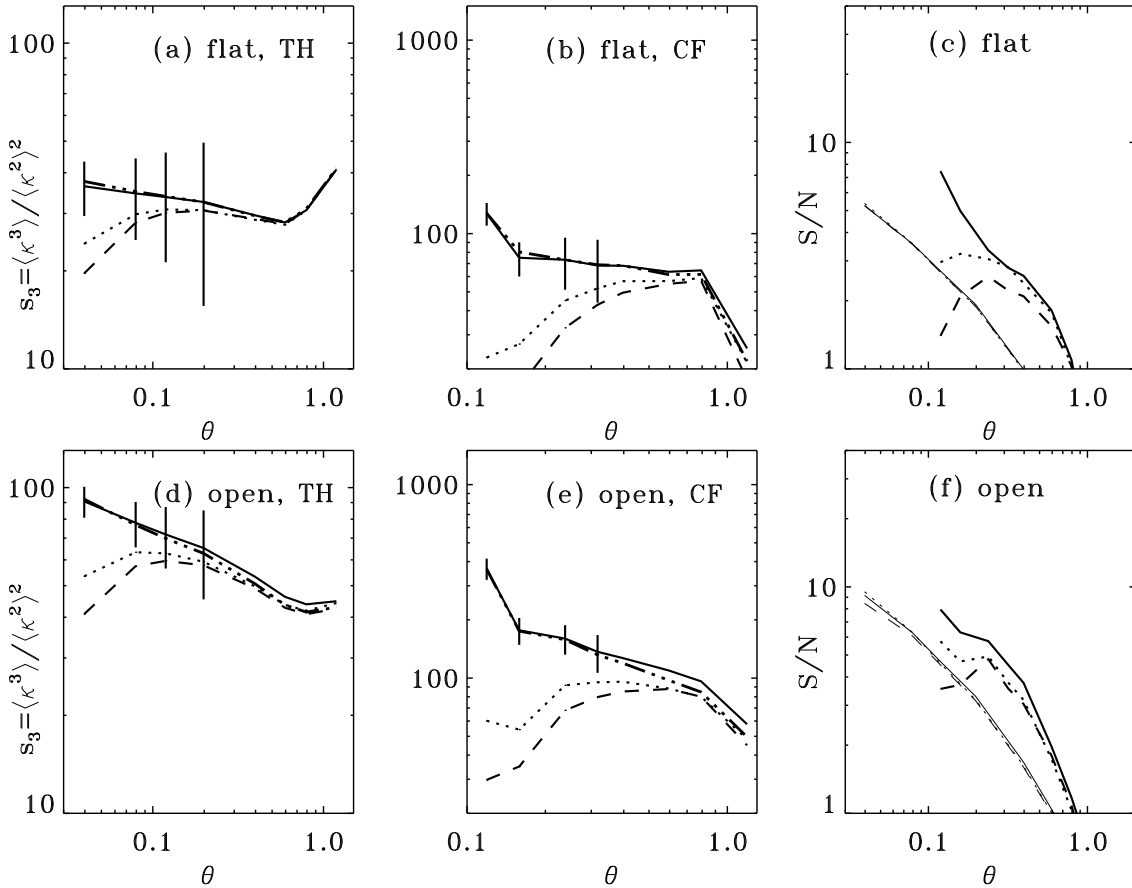


Fig. 8. Same as Fig. 7, but for the skewness of the convergence, s_3 .

ratio is 3 as expected from perturbation theory⁸, with a significance of the separation at roughly 6σ . This is observed in case of the top-hat as well as the compensated filter and this confirms the fact that the skewness of the convergence can strongly separate low and high density universes.

To be more precise we present the actual histograms of the measured skewness in Fig 9 which demonstrates clearly that the two cosmologies can be easily separated. One can see that the scatter in s_3 is roughly the same in the two cases and that the difference in the relative precision is due to the differences in the expectation values. This plot also shows that the distribution of the measured s_3 is quite Gaussian.

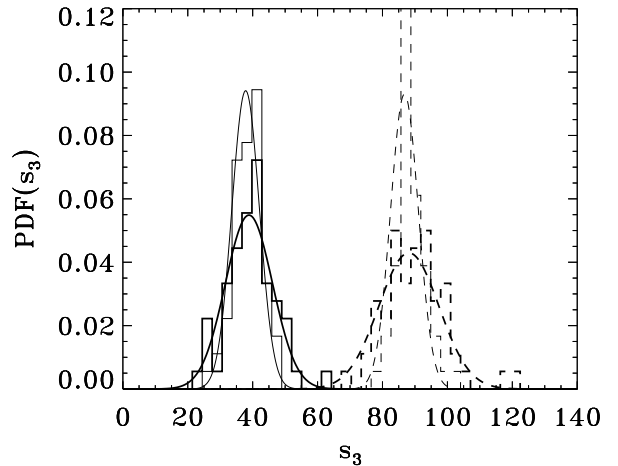


Fig. 9. Histograms of the values of s_3 , top-hat filter, for $\Omega = 1$ (solid lines) and $\Omega = 0.3$ (dashed lines) for a 5×5 degree survey (thick lines) and a 10×10 degree survey (thin lines). The angular scale is the pixel size $2.5'$.

⁸ To reduce the cosmic variance, we reject the pixel values that are above 4σ . It slightly reduces the value of s_3 for the open case.

4.5. Comparisons of different observational scenarios

The results presented previously had been obtained from the full mass reconstruction of 240 maps⁹ as described in Appendix B. Since it was demonstrated in the preceding section that noise acts as a pure de-correlated white noise in the reconstructed κ maps, we pursue our analyses of large series of simulated fields simply by adding the noise on the initial κ maps (especially for 10×10 degree data sets for which convergence reconstruction would take typically one and a half hour on DEC PWS-500 computers). The subsequent analysis are therefore made with this simplified scheme.

To complement the previous cases, we have built and analyzed the cosmic variance on 60 maps for each of the following models: open ($\Omega = 0.3$) and flat ($\Omega = 1$) cosmologies, a survey size of 5×5 degrees for $z_s = 1.5$, a survey size of 10×10 degrees for $z_s = 1$, with the power spectrum of Eq. (38) and a survey size of 5×5 for $z_s = 1$ with a CDM spectrum.

4.5.1. Effect of the survey size

By increasing the total area of a factor 4 we increase the signal to noise on the variance and the skewness with a top-hat filter by almost a factor 1.7. This can be seen in Fig. 9 when comparing the 5×5 degree case with the 10×10 case. With a compensated filter, the signal to noise ratios of the variance and of the skewness are increased by exactly a factor 2, thus improving more rapidly with the sample scale than the top-hat window function. This is expected from the de-correlation properties of those filters. It makes the compensated filter actually more attractive for such a large survey.

4.5.2. Effect of the source redshift

Fig. 10 shows the effect of a change in the mean source redshift. For the galaxies that are further away, the variance of κ is larger since the gravitational distortion is stronger, conversely the skewness is smaller since the accumulated material along the line of sight creates a field that is more and more Gaussian. The surprising result is that the signal to noise of these quantities does not depends strongly on the redshift of the sources. This means that it will be a waste of time to observe at high redshift, while it will basically not improve the precision of the measurement. Things are slightly improved for the compensated filter, but fundamentally, the results with the top-hat filter show that we do not learn more by increasing the redshift. Note that there is no improvement due to the increasing galaxy number density if the survey size is unchanged (see section 4.3). In addition, high redshift surveys may create new

problems such as uncertainties due to the Born approximation, the lens-lens coupling or the recently investigated source clustering effect (Bernardeau 1998).

4.6. BG versus CDM power spectrum

In order to test the robustness of the skewness as an estimator of Ω independent on the power spectrum we re-ran our simulations for a standard CDM power spectrum. Fig. 11 shows the comparison between the CDM model (dotted line) and BG power spectra, which clearly shows that CDM contains more structures at small scale by looking at the variance plots (a), (b). As predicted in BvWM, the skewness of the convergence is almost unaffected by the change of power spectrum (see Fig. 11 (d), (e)), but there is a small improvement in the signal to noise for the flat model (because of the larger power at small scale for CDM). On the other hand, the variance is strongly affected and in particular there is a significant decrease of power at large scale compare to BG spectrum. Note that the compensated filter yields a more accurate representation of the underlying power spectrum than the top-hat filter (because it is a pass band filter), and leaves the angular dependence of the variance unchanged compared to the spectrum Eq.(38) excepts at large scales.

The skewness is thus a robust estimator of Ω fairly insensitive to the power spectrum.

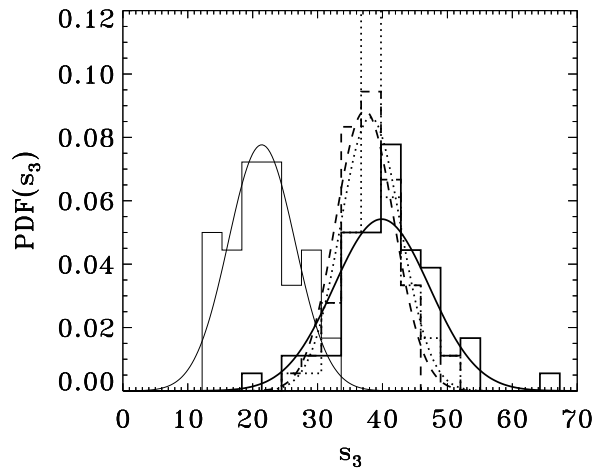


Fig. 12. Histograms of the values of s_3 for 5×5 degree survey, top-hat filter, for $\Omega = 1$ for a BG spectrum with $\sigma_8 = 0.6$ and $z_s = 1$ (thick solid line), $\sigma_8 = 0.6$ and $z_s = 1.5$ (thin solid line), $\sigma_8 = 1.0$ and $z_s = 1$ (dotted line) and a CDM spectrum with $\sigma_8 = 0.6$ and $z_s = 1$ (dashed line). The angular scale is the pixel size, $2.5'$.

⁹ This corresponds to the two noise levels for each cosmological model, with 60 mass maps for each case.

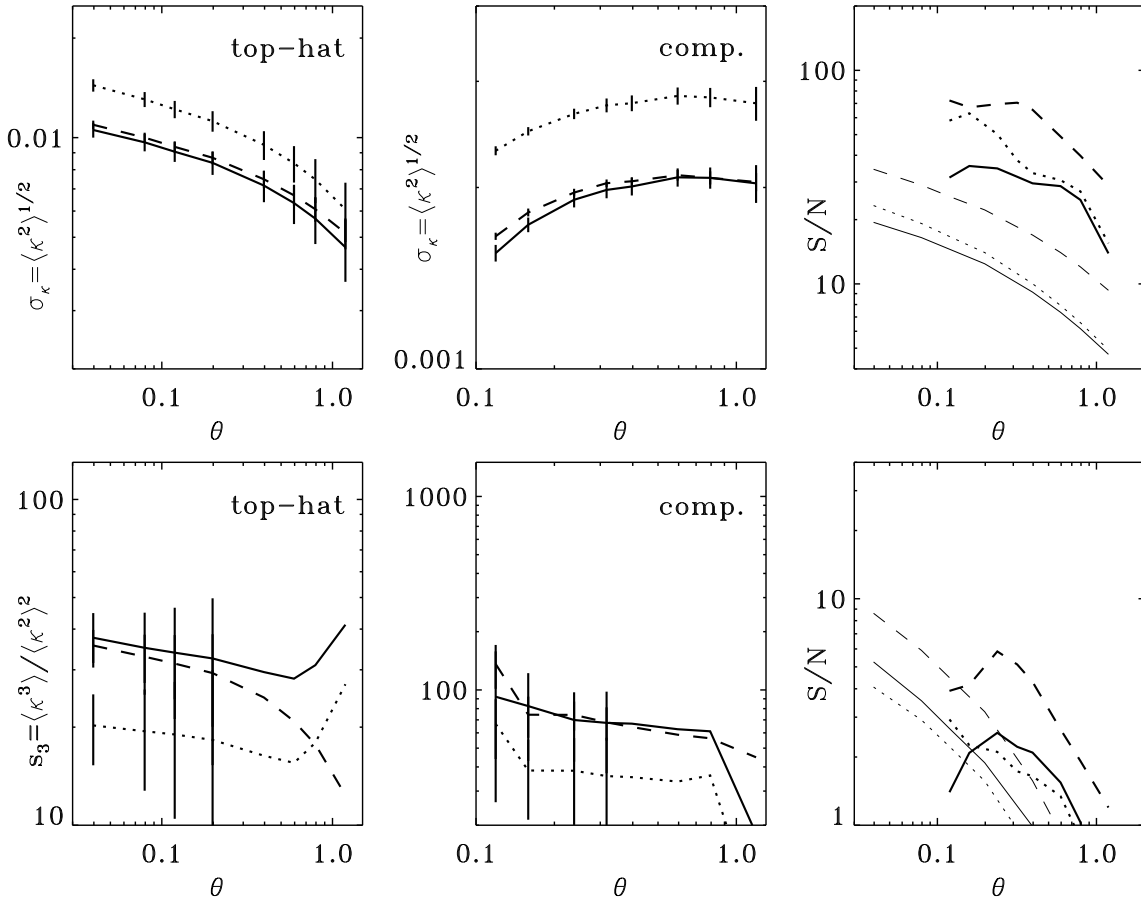


Fig. 10. For a flat cosmological model, comparison of different observational strategies between a survey of size 10×10 degrees (dashed lines) a 5×5 degrees survey for sources at mean redshift 1.5 (dotted lines) and a 5×5 degrees survey for sources at mean redshift 1 (solid lines). Left panels are for the top-hat filter and middle panels for the compensated filter. The thicker lines in the right panels hold for the compensated filter.

4.7. Effect of the normalization

The skewness s_3 is found to be independent on the normalization, as expected from the Perturbation Theory. The signal to noise ratio however is increased by about 40% in the case of high normalization $\sigma_8 = 1$. These results are summarized in Fig. 12 that shows the histograms for various cosmological cases. It demonstrates that the skewness is clearly independent on the shape and normalization of the power spectrum. However there is a strong dependence on the mean redshift of the sources. If the signal to noise ratio for s_3 depends on the cosmology it is independent on the mean source redshift. This again is favoring rather shallow surveys.

4.8. Beyond the skewness to measure Ω ?

The skewness of the PDF of the local convergence does not entirely characterize the PDF itself. Thus it is natural to measure higher order moments of the convergence to probe the cosmology.

It is clear that the skewness breaks the degeneracy between the power spectrum and the cosmological parameters, and is completely insensitive to the normalization. Bernardeau (1995) already noticed that in the case of cosmic density field or cosmic velocity field, the ratio s_4/s_3^2 calculated from the perturbation theory with a top-hat filter is almost a constant, and independent on the underlying cosmological model. This work was recently extended to the lensing case (Bernardeau, 1998) where he found $s_4(\kappa)/s_3(\kappa)^2 \simeq 2$. If all systematics of the gravitational lensing measurement can be controlled, search for such a *magic* number in our Universe would be a strong indication of validity of the paradigm of the gravitational instability scenario started from Gaussian initial conditions. On the other hand s_4 may be a new way to measure the density parameter (but not totally independent on the skewness). In our maps we find that the noise correction still works for the kurtosis, and that a compensated filter is more efficient than the top-hat filter (at least for noise-free data). In addition the kurtosis appears to be a fairly

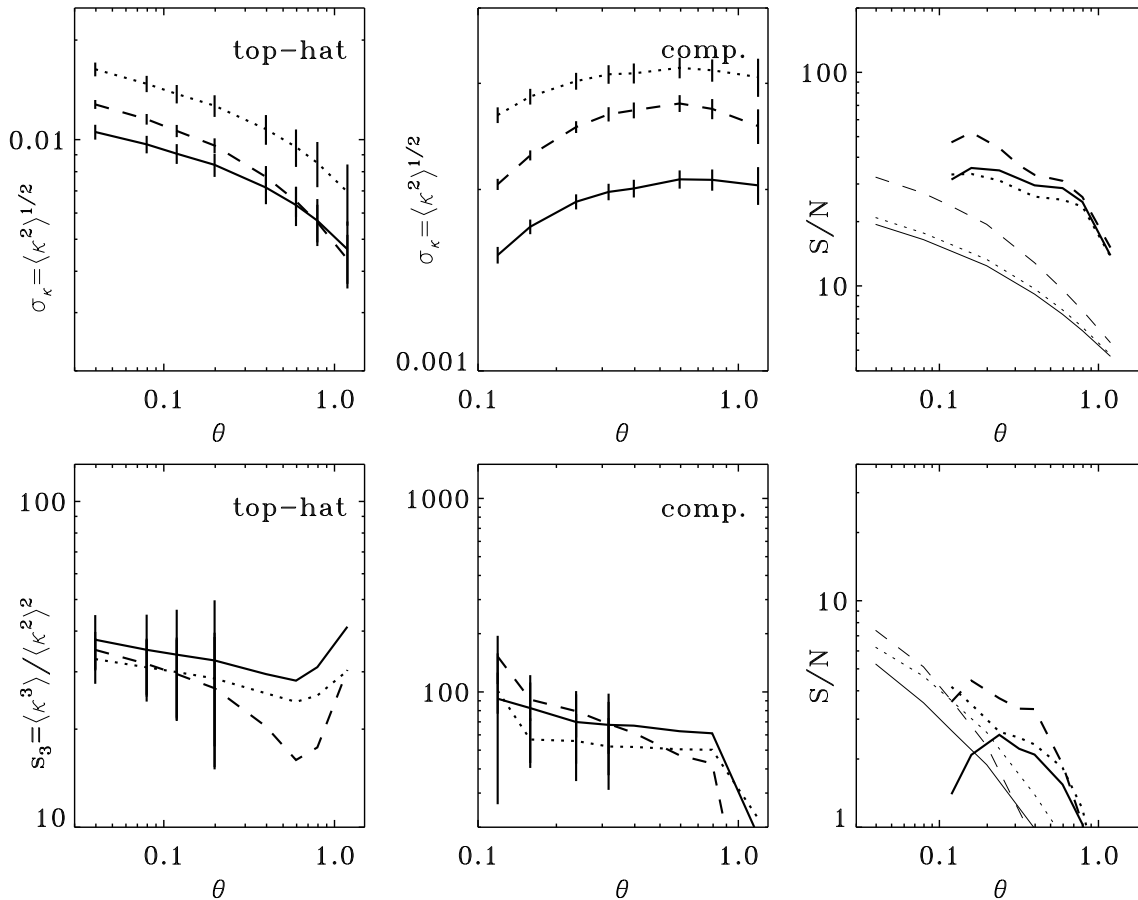


Fig. 11. Comparison of different choices of power spectra for a 5×5 degree survey and a flat cosmological model. The dashed lines correspond to an $\Omega = 1$ CDM spectrum with $\sigma_8 = 0.6$ and $z_s = 1$, dotted lines to a BG spectrum with $\sigma_8 = 1$ and $z_s = 1$, and the solid lines to a BG spectrum with $\sigma_8 = 0.6$ and $z_s = 1$.

good discriminant for Ω . Unfortunately the signal to noise ratio remains lower than for the skewness, which make it more difficult to measure. Moreover, it is more sensitive to the usual lensing approximations (Born approximation and lens-lens coupling terms) as well as source clustering (Bernardeau 1998). The error bars of the kurtosis found in our simulations are so large with a 5×5 degree survey that it is impossible to measure it at scales larger than a few arcminutes. It turns out that the ratio $s_4(\kappa)/s_3(\kappa)^2$ is ~ 1.4 for the flat case and ~ 1.8 for the open case for a top-hat filter, while it is ~ 5.6 for the flat case and ~ 3.4 for the open case for a compensated filter. It is not the scope of this work to compare further the differences between the two filters, but we want to point out that filtering may be an interesting way to change the dependence of an estimator versus the cosmology. This should be studied in order to search for optimal measurements of higher order moments. More generally, the whole shape of the PDF could probably be used with more efficiency than the skewness alone. In a regime of small departure from a Gaussian distribution it can for instance be fruit-

ful to describe the shape of the PDF with an Edgeworth expansion that takes into account the first few moments (Juszkiewicz et al. 1995, Bernardeau & Kofman 1995). For instance, from the Edgeworth expansion it is easy to show that the fraction of values of the convergence that is above the average value, $P(\kappa > \langle \kappa \rangle)$, is

$$P(\kappa > \langle \kappa \rangle) \approx \frac{1}{2} \left(1 - \frac{s_3 \sigma_\kappa}{6\sqrt{2\pi}} \right). \quad (25)$$

The results obtained from this formulae are in good agreement with those obtained from the direct measurements, however with a slightly larger cosmic variance.

Finally, the non-Gaussian features can also be characterized with topological indicators (which have been shown to be fruitful for the analysis if CMB data already, see for instance Winitzki & Kosowsky 1998, Schmalzing & Gorski 1997). What cosmic variance could be derived from the joint use of topological quantities or/and information on the shape of the PDF is left for further investigations.

5. Discussion

In this paper, we have focussed our investigations on scales larger than $2.5'$ thus allowing ourself the use of a simplified dynamics. This is a complementary approach to the ongoing investigations by Jain et al. (1998) who analyzed the high order moments and the power spectrum of the calculated from ray tracing in high resolution simulations. Although they only analyze the statistical properties of the convergence without noise, their approach completes our own towards the smaller angular scales. They have shown in particular that the skewness of the convergence is significantly higher at small scales (0.1 arcmin) than the theoretical expectations of perturbation theory due to highly non-linear structures, (this was already mentioned by Gaztañaga & Bernardeau 1998 and whether this behavior can still be described by means of perturbation theory with the help of loop correction terms is still an open question). Unfortunately, even at these small scales, they are not able to analyze the cosmic variance because of the small number of realizations. The use of high resolution simulations probably prevents a detailed analysis of this quantity.

The preceding sections provide quantitative estimates of the capability of mass reconstructions from weak lensing measurements at large scale to probe the large scale structures, as well as the cosmological parameters. We have shown how the projected mass distribution can be reconstructed accurately from the observed shape of the galaxies. Two complementary analysis have been examined, the power spectrum and the non-Gaussian features through the high order moments.

For the power spectrum estimation, the best sampling strategy (i.e. the question of sparse or compact surveys) is not discussed in this paper (see Kaiser 1998 for a discussion), but our results show that in order to probe the smallest scales of mass fluctuations a deep (but narrow) survey is required that diminishes the cosmic variance caused by the shot noise. Once this is done, the survey can be extended in a more shallower manner to probe the power spectrum at scale where the cosmic variance caused by shot noise becomes unimportant. At this stage, the question of a sparse or compact survey is a matter of choice, depending on scientific interests.

Concerning the moments measurement, a summary is given in Table 2 (for a top-hat filter) and 3 (for a compensated filter) which shows the smallest accessible error on the measurement of the variance and the skewness of the convergence for different observational contexts. This demonstrates that weak lensing measurements can reach a few percent precision on Ω for a reasonable survey size. We pointed out that the results are not much deteriorated for a number density of galaxies of 30 gal/arcmin^2 compared to 50 gal/arcmin^2 , whereas the realization of the survey in the latter case requires a factor 3 more observing time. It suggests that large shallow surveys would be more ade-

Table 2. Relative error on the measured variance and skewness of the convergence in different observational contexts (in tables $n_1 = 30 \text{ gal/arcmin}^2$ and $n_2 = 50 \text{ gal/arcmin}^2$) for a top-hat filter. The numbers correspond to the smallest error within the range of scales considered in this work.

Observational constraints		$\Omega = 1$		$\Omega = 0.3$	
		$\delta\sigma_\kappa/\sigma_\kappa$	$\delta S_3/S_3$	$\delta\sigma_\kappa/\sigma_\kappa$	$\delta S_3/S_3$
$5 \times 5 \text{ deg}$ $z_s = 1$	n_1	0.051	0.190	0.047	0.118
	n_2	0.050	0.186	0.047	0.105
$5 \times 5 \text{ deg}$ $z_s = 1.5$	n_1	0.043	0.246	0.038	0.127
	n_2	0.043	0.223	0.038	0.123
$10 \times 10 \text{ deg}$ $z_s = 1$	n_1	0.029	0.116	0.024	0.060
	n_2	0.029	0.110	0.023	0.054

Table 3. Same as Table 2 for a compensated filter

Observational constraints		$\Omega = 1$		$\Omega = 0.3$	
		$\delta\sigma_\kappa/\sigma_\kappa$	$\delta S_3/S_3$	$\delta\sigma_\kappa/\sigma_\kappa$	$\delta S_3/S_3$
$5 \times 5 \text{ deg}$ $z_s = 1$	n_1	0.028	0.391	0.044	0.209
	n_2	0.021	0.310	0.043	0.174
$5 \times 5 \text{ deg}$ $z_s = 1.5$	n_1	0.016	0.341	0.030	0.193
	n_2	0.016	0.310	0.029	0.172
$10 \times 10 \text{ deg}$ $z_s = 1$	n_1	0.014	0.171	0.020	0.110
	n_2	0.014	0.140	0.020	0.074

quate since it efficiently reduces the cosmic variance. Such a strategy would be much more comfortable with respect to some systematics like the redshift distribution of the sources (which can be determined easily if the sources are closer), the source clustering effects that are limited if the source distribution is narrow (Bernardeau 1998), and possibly the morphological evolution of distant galaxies, in particular if most distant galaxies are composed of many merging substructures.

Note that there is still room for potential improvement of the signal to noise ratio we are obtaining. Indeed, since we are limited by construction to simulations of scales larger than $2.5'$ we do not know whether the cosmic variance can be reduced by observing the moments at smaller scales, as it is suggested by the results obtained with a top-hat filter (for which the signal to noise curves never bend down at small scales). The optimal size for the measurement of the variance and the skewness might in fact correspond to the arcmin scale. However, there are several issues that are generally believed to be irrelevant for weak lensing at large scales, but are probably potential difficulties at small scales:

- Our work implicitly assumes a constant power spectrum below the pixel size. A mass reconstruction from real data should include small scale features such as cluster lensing, and the propagation of the noise from this peaks of signal is not known. Moreover that abil-

ity of the χ^2 method to match the noise properties correctly at small scales should be reinvestigated.

- Born approximation and lens-lens coupling terms are stronger at small scales (see SvWJK). A quantification of this effect on simulations would be necessary to decide at which scale the measurement of moments is optimal.
- Source clustering (investigated at large scales by means of perturbation theory by Bernardeau 1998) could also have a significant impact at small scale.

The possible systematics caused by all these effects have to be investigated in order to estimate the precision of weak lensing surveys.

Moreover the moments are not necessary the *best* means to distinguish between different cosmological models (not to mention the fact that the results are anyway sensitive to the choice of the filter). For example, it seems that by comparing open and flat universes on Fig. 1 topological tools should be as well a strong discriminant of cosmological models. The statistical instruments are extremely diverse. Among the possible tools the results of multi-scale filtering, as provided by wavelet transforms, is likely to be a good candidate.

6. Conclusion

We have investigated in detail how weak lensing observations could be used to measure the projected power spectrum and to discriminate among different cosmological models. In order to analyze the cosmic variance of the results (which requires a large number of realizations), we used a two dimensional, second order Lagrangian dynamics to generate the convergence fields. In each of the observational situation and cosmological model, 60 different maps has been generated. Cosmological models include: flat model ($\Omega = 1$), open model ($\Omega = 0.3$), Baugh & Gaztañaga initial power spectrum, standard CDM spectrum. Observational contexts include: high noise (30 gal/arcmin²) and low noise (50 gal/arcmin²) level, "small" survey size (5 × 5 degrees) and large survey size (10 × 10 degrees), two different mean redshift of the sources ($z_s = 1$ and $z_s = 1.5$), and the use of top-hat and compensated filters. From these convergence maps, a shear map is calculated, on which the noise is introduced according the selected observational context, the mass map is finally reconstructed (using a χ^2 method) and analyzed.

Our results are:

- At scales larger than 2.5' the χ^2 reconstruction method is a very stable process which does not produce any boundary effects, spurious signal, and which leaves the noise properties unchanged (the noise does not propagates and remains close to the theoretical prediction using the linearized lens equation). This permits to work with the convergence (which is the physical field

of interest) instead of the shear, with no loss of information.

- The shot noise contribution can be removed simply by measuring the *observed* ellipticities of the galaxies, and this leads to unbiased estimates of the power spectrum and the moments of the convergence (at least up to the kurtosis).
- The precision obtained on the normalization can be as low as 2% with survey of 10 × 10, and 5% for Ω (see tables 1 and 2) for the most favorable cases (i.e. low Ω).
- The larger shallower surveys are more promising to recover the cosmological quantities. In addition to that, the redshift distribution of the brighter galaxies is known better and their light distribution is more regular, making ellipticity measurement from their weighted second moment easier and more relevant.
- The compensated filter yields by far smaller cosmic variance than the top-hat filter for the variance of the convergence, while it gives unsatisfactory results for the skewness. However the cosmic variance decreases more rapidly with an increasing survey size for a compensated filter.

The MEGACAM project offers the possibility to perform these observations. Indeed the large field of the CCD device (1 square degree) and the high image quality at CFHT (extended to the edges of the field with the future field corrector) provides the ideal instrument to perform such a scientific program.

In the context of the rapid changes occurring in observational cosmology it is worth stressing that weak lensing surveys offer precious complementary views of our Universe and unique tools to probe *directly* the dark matter and to compare with the light distribution at any scales. The perspective of determining the projected power spectrum independently of biases is indeed attractive. Moreover the possibility of determining Ω_0 in a way which is independent on the power spectrum, and independent on all the methods that have been suggested so far, is also extremely precious. We remind that this determination relies only on dynamical effects assuming that the large-scale structures originate from Gaussian initial conditions through gravitational instabilities. In Fig. 13 examples of constraints in the (Ω, λ) plane with weak lensing as describes in this work (shaded areas) are presented¹⁰ together with the location of the major constraints that are expected to be brought either with CDM experiments, (constant curvature density, solid lines), or from Type-Ia supernovae measurements (the other straight lines, describing constant q_0 values).

Future CMB experiments can determine the cosmological parameters with a remarkable accuracy, but only when some prior is put on the shape of the initial power spec-

¹⁰ The λ dependence is taken from the theoretical results given by BvWM.

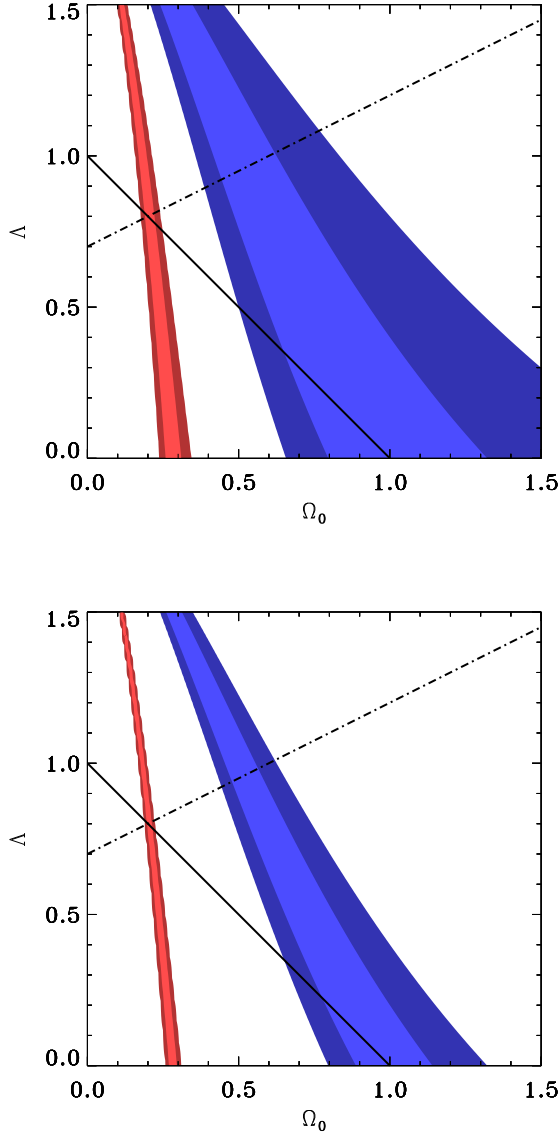


Fig. 13. Constraints that can be brought by weak lensing survey in an $\Omega_0 - \lambda$ plane. The grey areas are the location of the 1 and 2- σ bands (respectively darker and lighter bands) allowed by a measured skewness that would be obtained with either $\Omega_0 = 0.3$ (left bands) or $\Omega_0 = 1$ (right bands). The solid straight lines corresponds to a zero curvature universe, and the dot-dashed lines to a fixed acceleration parameter, q_0 . The panels correspond to survey of either 5×5 (top) or 10×10 degrees (bottom).

trum. The curvature will probably be determined with a good accuracy in the near future from the position of the first Doppler peak on the C_l curves. But it appears that it can be very difficult to disentangle Ω_0 from λ (see for instance Zaldariagga, Spergel & Seljak 1997) from the mere temperature (and polarization) fluctuations. This might be only possible from a very detailed analyses and the power spectra which require not only a good understanding of the possible systematics that may affect the measurements, but also specific hypothesis on the regularity of the primordial power spectrum. The requirements to measure Ω_0 from weak lensing survey are less strict provided the instrumental systematics can be controlled correctly.

Moreover weak lensing surveys are able to constraint λ if it is possible to select efficiently several populations of sources (see Villumsen 1996, BvWM for clues of such possibilities). We thus think that weak lensing survey will be a major mean for probing the global cosmological parameters. It is complementary to the CMB experiments and indispensable for breaking the parameter degeneracy.

The feasibility of the weak lensing by large scale structure program and The full scientific exploitation of the weak lensing effect is reduced to the capability to control instrumental systematics, where there are still open crucial points. The most dedicated problem comes probably from the need of a PSF correction able to avoid artificial large scale coherent alignments of galaxies. Related to this problem is the pixelisation effect. Galaxies shapes are indeed determined from a finite number of pixels with the possible introduction of errors and biased estimation on the shapes.

These effects can all be investigated independently. Taking several images of the same portion of the sky with a shifted position for the camera, or with different cameras would definitely test the robustness of the observed distortion maps. Moreover we have numerous statistical tests at our disposal that can be done on the maps: comparison of the 2-point correlation function of the distortion with the one of the shear field or with the one of the κ field, or even by the investigation of quantities that are a priori sensitive to the systematics in a different manner, such as the correlation of the orientations of the distortion field. That all these quantities have related properties is somehow due to the fact that in the thin lens approximation the γ field should be curl-free (see for example Luppino & Kaiser 1997 for a used of these tests). This is true only when lens-lens couplings are neglected but it should be possible to investigate those effects in numerical simulations.

Acknowledgements. It is a pleasure to thanks S. Colombi for his useful suggestion to use a second order Lagrangian dynamics, B. Fort, P. Schneider, B. Jain and U. Seljak for fruitful discussions. We are very greatfull to the referee S. Seitz for her extremely detailed report with very useful remarks and suggestions. This research has been conducted under the auspices

of a European TMR network programme made possible via generous financial support from the European Commission. This work was also supported by the Programme National de Cosmologie and the ‘‘Sonderforschungsbereich 375-95 f ur Astro-Teilchenphysik’’ der Deutschen Forschungsgemeinschaft. L.V.W. and F.B. thank IAP, where a fair fraction of this work has been done, for hospitality.

References

- Bartelmann M., Narayan R., Seitz S., Schneider P. 1996, ApJ 464, 115
- Baugh C. M., Gazta naga E. 1996, MNRAS 280, L35
- Bernardeau F. 1998, A&A accepted, astro-ph/9712115
- Bernardeau F. 1995, A&A 301, 309
- Bernardeau F., Kofman L. 1995, ApJ 443, 479
- Bernardeau F., Singh T.P., Banerjee B., Chitre S.M. 1994, MNRAS 269, 947
- Bernardeau F., Van Waerbeke L., Mellier Y. 1997, A&A 322, 1
- Blandford R. D., Saust A. B., Brainerd T. G., Villumsen J. V. 1991, MNRAS 251, 600
- Bonnet H., Mellier Y. 1995, A&A 303, 331
- Bouchet F., Colombi S., Hivon E., Juszkiewicz R. 1995, A&A 296, 575
- Bouchet F., Colombi S., Juszkiewicz R., Pellat R. 1992, ApJ 394, L5
- Boulade O., Vigroux L., Charlot X., et al. 1998, ‘‘MEGACAM, the next Generation Wide-Field camera for CFHT’’. SPIE Vol. 3355, ‘‘Astronomical Telescopes and Instrumentation’’, Kona Hawaii, March 1998
- Colombi S., Bernardeau F., Bouchet F., Hernquist L. 1997, MNRAS 287, 241
- Colombi S., Szapudi I., Szalay A. 1998, MNRAS 296, 253
- Eke V., Cole S., Frenk C. 1996, MNRAS 282, 263
- Feldman H. A., Kaiser N., Peacock J. A. 1994, ApJ 426, 23
- Gazta naga E., Bernardeau F. 1998, A&A 290, 566
- Gunn J.E., 1967, ApJ 150, 737
- Jain B., Seljak U., White S.D.M., astro-ph/9804238
- Jaroszyński M., Changbom P., Paczyński B., Gott J.R. 1990, ApJ 365, 22
- Juszkiewicz R., Weinberg D., Amsterdamski P., Chodorowski M., Bouchet F.R., 1995, ApJ 442, 39
- Kaiser N. 1992, ApJ 388, 272
- Kaiser N. 1995, ApJ 439, L1
- Kaiser N., Squires G., Broadhurst T. 1995, ApJ 449, 460
- Kaiser N. 1998, ApJ 498, 26
- Luppino G., Kaiser N. 1997, ApJ 475, 20
- Oukbir J., Blanchard A. 1997, A&A 317, 1
- Moutarde F., Alimi J.M., Bouchet F., Pellat R., Ramani A. 1991, ApJ 382, 377
- Munshi D., Bernardeau F., Mellot A.L., Schaeffer R. 1997, astro-ph/9707009
- Munshi D., Sahni V., Starobinsky A.A. 1994, ApJ 436, 517
- Seljak U. 1997, astro-ph/9711124
- Schmalzing J., Gorski K. M., astro-ph/9710185
- Schneider P., Seitz C. 1995, A&A 294, 411
- Schneider P., Van Waerbeke L., Jain B. Kruse, G. 1997, MNRAS accepted, astro-ph/9708271 (SvWJK)
- Schramm T., Kayser R. 1995, A&A 299, 1
- Seitz S., Schneider P., Bartelmann M. 1998, astro-ph/9803038
- Squires G., Kaiser, N. 1996, ApJ 473, 65
- Stebbins A. 1996, astro-ph/9609132
- Szapudi I., Colombi S. 1996, ApJ, 470, 131
- Van Waerbeke L., Mellier Y., Schneider P., Fort B., Mathez G., A&A 317, 303
- Villumsen, J.V., 1996, MNRAS 281, 369
- Winitzki S., Kosowsky A., astro-ph/9710164
- Zel’dovich Y. B. 1970, A&A 5, 84

Appendix A: Second order Lagrangian dynamics

In order to investigate the statistical properties of the reconstructed mass field that contains a significant amount of non-linearities, a non-linear evolution model of large-scale structures is required. Second order Lagrangian perturbation theory has the advantage to be extremely fast to compute, and rather accurate compared to N-body simulations. It gives correct values for the skewness S_3 and we expect it to give correct estimation of the cosmic variance (see Munshi et al. 1994, Bernardeau et al. 1994, Bouchet et al. 1995).

Actually we do not even need to do 3D simulations. At the level of perturbation theory it is equivalent to perform 2D second order Lagrangian evolutions of the structures on an initial linear map of the projected mass fluctuations.

Construction of the initial linear map

The local convergence map is given by

$$\kappa(\varphi) = -\frac{3}{2} \Omega_0 \int_0^{\chi_H} d\chi_s n(\chi_s) \int_0^{\chi_s} d\chi \frac{\mathcal{D}_K(\chi_s - \chi) \mathcal{D}_K(\chi)}{\mathcal{D}_K(\chi_s)} \frac{\delta(\mathcal{D}_K(\chi)\varphi, \chi)}{a}, \quad (26)$$

where χ_H is the horizon distance, Ω_0 the density parameter, a the expansion factor and $n(\chi_s)$ the number density of sources as a function of the distance χ . For clarity we introduce the lens efficiency function

$$w(\chi) = \frac{3}{2} \Omega_0 \int_\chi^{\chi_H} d\chi_s n(\chi_s) \frac{\mathcal{D}_K(\chi_s - \chi) \mathcal{D}_K(\chi)}{a \mathcal{D}_K(\chi_s)}, \quad (27)$$

so that the local convergence is simply given by the integral over the line of sight of,

$$\kappa(\varphi) = - \int_0^{\chi_H} d\chi w(\chi) \delta(\mathcal{D}_K(\chi)\varphi, \chi). \quad (28)$$

The projected density contrast would be,

$$\delta_{2D} = \frac{\kappa}{\bar{w}} \quad \text{with} \quad \bar{w} = \int_0^{\chi_H} d\chi w(\chi). \quad (29)$$

It is important to keep in mind that the local convergence is related to the actual density contrast with a constant that depends on the cosmological parameters. In the following we will assume that all sources are at the same

redshift (it is not realistic but of no consequences on our results here).

In the linear approximation the κ field is expected to be a 2D Gaussian field, characterized by a power spectrum, P_κ , with (see Kaiser 1992, 1996, and SvWJK)¹¹,

$$P_\kappa(\mathbf{k}) = \int_0^{\chi_H} d\chi w(\chi)^2 P_\delta\left(\frac{\mathbf{k}}{\mathcal{D}_K(\chi)}, \chi\right), \quad (30)$$

as a result of the relation between κ and the 3D density contrasts. The initial conditions for κ are therefore generated by a 2D Gaussian field in Fourier space where the complex random variables verify

$$\langle \tilde{\kappa}(\mathbf{k}) \tilde{\kappa}^*(\mathbf{k}') \rangle = (2\pi)^2 \delta_D(\mathbf{k} - \mathbf{k}') P_\kappa(\mathbf{k}), \quad (31)$$

The 2D second order Lagrangian dynamics

In order to introduce a significant amount of nonlinearities in the maps, we apply the 2D second order Lagrangian dynamics to the projected density, δ_{2D} . Following the notations of Bouchet et al. (1992), transposed in the 2D case, let us write the 2D Eulerian coordinates $\boldsymbol{\theta}(\mathbf{q})$ as a perturbation series over the 2D displacement field \mathbf{D} ,

$$\boldsymbol{\theta}(\mathbf{q}) = \mathbf{q} + \epsilon \mathbf{D}^{(1)}(\mathbf{q}) + \epsilon^2 \mathbf{D}^{(2)}(\mathbf{q}) + o(\epsilon^3), \quad (32)$$

where \mathbf{q} is the angular Lagrangian coordinate and ϵ a small dimension-less parameter. The first order term reduces to the Zel'dovich (Zel'dovich 1970) approximation. The divergence of the second order displacement field can be written in terms of the first order solutions,

$$\mathbf{D}_{i,i}^{(2)}(\mathbf{q}) = \frac{3}{7} \left[\mathbf{D}_{1,1}^{(1)} \mathbf{D}_{2,2}^{(1)} - \left(\mathbf{D}_{1,2}^{(1)} \right)^2 \right]. \quad (33)$$

This result is exact for an Einstein-de Sitter Universe. The values of the coefficient 3/7 is only slightly altered (about 1%) for other cosmological models (Bouchet et al. 1992, Bernardeau 1994) and in the following we did not take into account this dependence. Once the second order displacement field has been computed, the local 2D density contrast can then be written in terms of the Jacobian of the transform between the Lagrangian coordinates and the Eulerian coordinates,

$$\delta_{2D}(\boldsymbol{\theta}(\mathbf{q})) = \frac{1}{J(\mathbf{q})} \quad (34)$$

where $J = |\partial\theta_i/\partial q_j|$. The local convergence is then given by

$$\kappa(\boldsymbol{\theta}(\mathbf{q})) = \bar{\omega} \delta_{2D}(\boldsymbol{\theta}(\mathbf{q})). \quad (35)$$

The linear density maps are built on a regular grid from random modes following a given power spectrum. The different quantities up to the Jacobian are generated on this

¹¹ Taking $H_0 = c = 1$.

same grid by successive Fast Fourier Transforms. There is then a technical difficulty to solve in order to get the resulting values of κ on a regular grid. This is done via a local triangulation and an interpolation of the values (from standard IDL packages). Note that the continuity equation provides us with κ and not with the projected potential. The latter will have to be computed from a subsequent Fourier transform (see Appendix B). The amplitude of the fluctuations is such that the displacement field does not induce shell crossings¹². Finally, bands of sufficient width along the edges were cut out to avoid edge effects induced by the displacement field.

The skewness with this approximate dynamics

The skewness of the projected density is given by the skewness of the 2D dynamics (Munshi et al. 1997), that is,

$$s_3^{\text{density}} = \frac{36}{7} + \frac{3}{2} \frac{d \log \sigma^2(\theta)}{d \log \theta}. \quad (36)$$

The skewness for the convergence would then simply be

$$s_3^{\text{convergence}} = \frac{1}{\bar{\omega}} \left(\frac{36}{7} + \frac{3}{2} \frac{d \log \sigma^2(\theta)}{d \log \theta} \right). \quad (37)$$

This result has to be compared with the results obtained in BvWM. Their general formula (67) contains some extra geometrical factors of order unity (coming from a different averaging procedure along the line of sight). Eq. (37) actually corresponds to the approximate form of Eq. (75) of BvWM.

Shapes and normalizations of the power spectra

The 3D power spectrum given by Baugh & Gaztañaga (1996) (BG spectrum) is used in most of our simulations,

$$P(\mathbf{k}) \propto \frac{k}{[1 + (k/k_c)^2]^{3/2}}, \quad (38)$$

where $k_c = 0.05 h_{100} \text{Mpc}^{-1}$. In a series of simulations we compared this model also with the standard CDM spectrum.

In most cases the fluctuations are normalized according to the convergence field $\sigma_\kappa = Cste$. The value of σ_8 that has been chosen thus depends on Ω_0 in such a way that it is equal to 0.6 for a flat Universe (following the normalization inferred from galaxy cluster counts (Eke et al. 1996, Oukbir & Blanchard 1997)). As a result we take,

$$\sigma_8 = 0.6 \frac{\bar{\omega}(\Omega_0 = 1)}{\bar{\omega}(\Omega_0)} \quad (39)$$

¹² However, in the open cases it very rarely happened that κ reached unrealistic large values. The amplitude of κ has therefore been arbitrarily limited to 0.1. At most a handful of pixels have been affected by this cut-off.

It implies that the value of σ_8 grows for low values of Ω . Note that since $\bar{\omega} \approx \Omega^{-0.8}$, this growth is only slightly more important in our case than for the galaxy cluster counts (the exponent would be about 0.5 to 0.6).

Appendix B

This appendix gives the details of the reconstruction algorithm, how the g map is generated from an initial κ map, and the noise model.

Reconstruction algorithm

The lensing quantities of interest are defined in the Eqs.(6), and the observable is the reduced shear $g = \gamma/(1 - \kappa)$. The reconstruction problem is how to infer the κ map from an observed ellipticity field ϵ_{obs} , knowing that $\langle \epsilon_{obs} \rangle = g$ is an unbiased estimate of the reduced shear? Note that this problem is under-constrained since a change in the potential ψ of the form,

$$\psi \rightarrow \lambda\psi + \frac{(1 - \lambda)}{2} |\boldsymbol{\theta}|^2, \quad (40)$$

where λ is a constant, leaves the reduced shear g invariant, but will transform the convergence as $\kappa \rightarrow \lambda\kappa + 1 - \lambda$ (see Seitz et al. 1998). This is the so called mass-sheet degeneracy. Thus in order to get a realistic convergence map, λ has to be determined by forcing $\bar{\kappa} = 0$ at the survey scale. The estimate of κ is obtained by a non-parametric least χ^2 method (Bartelmann et al. 1995). The image is sampled on a $N \times N$ grid, and the potential on a $(N + 2)^2$ grid. Starting from a guess on ψ , a guess on the reduced shear is obtained and the following function is minimized with respect to ψ ,

$$\chi^2 = \sum_{ij} |g(\psi) - g|^2. \quad (41)$$

The finite difference schemes which are used in order to calculate the second derivatives of the potential at pixel (i, j) are,

$$\begin{aligned} \psi_{11}(i, j) &= [\psi(i + 2, j) + \psi(i - 2, j) - 2\psi(i, j)] / 4\Delta^2 \\ \psi_{22}(i, j) &= [\psi(i, j + 2) + \psi(i, j - 2) - 2\psi(i, j)] / 4\Delta^2 \\ \psi_{12}(i, j) &= [\psi(i + 1, j + 1) - \psi(i + 1, j - 1) \\ &\quad - \psi(i - 1, j + 1) + \psi(i - 1, j - 1)] / 4\Delta^2, \end{aligned} \quad (42)$$

where Δ is the pixel size. We found that these schemes give the best regularization at small scales and avoid the usual high frequency oscillations in crude reconstruction schemes. At the edges of the field the shift of 2 pixels in Eqs. (42) must be only one pixel in the direction perpendicular to the border since the potential is sampled on a $(N + 2)^2$ grid only. This has the consequence to slightly increase the noise at the boundaries but does not produce any bias. Once Eq. (41) is minimized, the κ map is found, and then the condition $\bar{\kappa} = 0$ is imposed on it.

Construction of the initial g map

A problem that we have to solve in this work is how to get the shear pattern of a projected mass distribution? Namely from the simulated κ we want to get the corresponding distortion map, put a noise on it, and reconstruct κ . The construction of a distortion map from a convergence map is unfortunately an under-constrained problem again. For example any transformation of the potential $\psi \rightarrow \psi + \bar{\psi}$ with $\Delta\bar{\psi} = 0$ leaves the convergence unchanged, but may change the shear (such a solution is for example $\theta_x^2 - \theta_y^2 + \theta_x\theta_y$). A peculiar solution for the potential ψ can be obtained by minimizing the χ^2 function:

$$\chi^2 = \sum_{ij} (\kappa - \kappa_{\text{guess}})^2. \quad (43)$$

The resulting reduced shear is then $g + \bar{g}$, where \bar{g} is the unphysical solution given by $\bar{\psi}$, but it is possible to reconstruct the convergence using Eq.(41), since κ is unchanged by the presence of the term \bar{g} . Unfortunately it is no longer the case when the noise is included via Eq.(10), because \bar{g} explicitly comes in the denominator. Fortunately, the role of the denominator in Eq.(10) is weak (this is a one percent effect on each galaxy if we take $g \simeq \bar{g} \simeq 0.01$ and $\epsilon^{(s)} \simeq 0.1$), this is in particular one of the reasons why the weak lensing approximation works so well. We thus did not try to correct for the presence of a spurious contribution \bar{g} in all the calculations, since it gives a negligible contribution to the signal (in terms of power spectrum and moments).

Noise generation

Once the true g maps are obtained the noise is introduced in a realistic way, using Eq.10: a sample of background galaxies with random intrinsic orientations is sheared, from which the κ map is reconstructed. The galaxies are observed in a grid of *superpixels* of 2.5 arcmin size (the minimum size of the κ map simulations), in which the number of galaxies N_i per superpixel i is known. In principle this number suffers of the amplification bias (depending on the line of sight matter quantity), but this effect is neglected here. N_i follows a Gaussian distribution of mean N_p and variance $\sqrt{N_p}$. Each pixel i of the image gives a local estimate of the reduced shear from the N_i galaxies, each of them having an intrinsic ellipticity $\epsilon_j^{(s)}$ which contributes as a source of noise for the shear signal. The distribution of $\epsilon_j^{(s)}$ is a truncated normalized Gaussian defined over the range $[0, 1]$,

$$p(\epsilon_j^{(s)}) \propto \exp\left(-\left(\frac{\epsilon_j^{(s)}}{\sigma_\epsilon}\right)^2\right), \quad (44)$$

where we choose $\sigma_\epsilon = 0.12$. (which corresponds to a typical axis ratio of 0.8).

From Eq. (10), the observed mean ellipticity $\bar{\epsilon}_i$ of a number N_i of galaxies in the image plane is given by

$$\bar{\epsilon}_i = \frac{1}{N_i} \sum_{j=1}^{N_i} \frac{\epsilon_j^{(s)} - g}{1 - g^* \epsilon_j^{(s)}}. \quad (45)$$

Where $\bar{\epsilon}_i$ is an unbiased estimate of the reduced shear g in the superpixel i (Schramm & Kayser 1995, Schneider & Seitz 1995). A realistic estimate of N_p depends on the observational context, the telescope used, the optical filter, the atmospheric conditions. By choosing $N_p = 30$ gal/arcmin² or 50 gal/arcmin² we adopted a conservative and reasonable assumption about the telescope time: the former is accessible in the I-band with 1.5 hour integration at CFHT, while the later is accessible for 4 hours in the same conditions.